博士論文

患者由来 iPS 細胞を用いた FTDP-17 タウ R406W 変異の病態モデル構築と病態解析

中　村　真　理

患者由来 iPS 細胞を用いた FTDP-17 タウ R406W 変異の病態モデル構築と病態解析

東京大学大学院　医学系研究科

国際保健学専攻　生物医化学教室

指導教員：渡邊　洋一

氏名：中村　真理

Table of content

Abbreviations

Aβ	amyloid-beta
AD	Alzheimer`s disease
AP	alkaline phosphatase
APP	amyloid beta precursor protein
ATP	adenosine triphosphate
bFGF	basic fibroblast growth factor
CDK5	cyclin-dependent kinase 5
cDNA	complementary deoxyribonucleic acid
CMV	cytomegalovirus
CRISPR/Cas9	clustered regularly interspaced short palindromic repeats/CRISPR associated protein 9
DNA	deoxyribonucleic acid
DMEM	Dulbecco's Modified Eagle's Medium
DTT	dithiothreitol
EB	embryonic body
EBNA1	Epstein–Barr nuclear antigen 1
EDTA	ethylenediaminetetraacetic acid
EpoD	epothilone D

ESC	embryonic stem cell
eGFP	enhanced green fluorescent protein
eYFP	enhanced yellow fluorescent protein
FOXG1	forkhead box protein G1
FTDP-17	frontotemporal dementia and parkinsonism linked to chromosome 17
GAPDH	glyceraldehyde-3-phosphate dehydrogenase
GSK3β	glycogen synthase kinase 3β
GST	glutathione S-transferase
HEPES	4-(2-hydroxyethyl)-1-piperazineethanesulfonic acid
iPSC	induced pluripotent stem cell
ITR	inverse terminal repeat
kb	kilobase
KLF4	Kruppel-like factor 4
KSR	Knockout Serum Replacement
MAPT	microtubule associated protein tau
MAP2	microtubule associated protein 2
MEF	mouse embryonic fibroblast
$MgCl_2$	magnesium chloride
MT	microtubule

MTBD	microtubule binding domain
NaCl	sodium chloride
NaF	sodium fluoride
NEAA	non-essential amino acids
NFT	neurofibrillary tangle
NP-40	nonyl phenoxypolyethoxylethanol
OCT3/4	octamer-binding transcription factor 3/4
PBMC	peripheral blood mononuclear cell
PBS	phosphate saline buffer
PCR	polymerase chain reaction
PGK	phosphoglycerate kinase
PHF	paired helical filament
PKA	protein kinase A
PRGN	progranulin
PSEN1	presenilin 1
PSEN2	presenilin 2
qRT-PCR	quantitative real-time polymerase chain reaction
RhoK	Rho-associated protein kinase
SDS-PAGE	sodium dodecyl sulfate-polyacrylamide gel electrophoresis

sgRNA	single-guide ribonucleic acid
SOX2	SRY-box 2
TBR1	T-box brain protein 1
TK	thymidine kinase
WT	wild-type

Abstract

Genetic mutations in the microtubule-associated protein tau (*MAPT*) gene are known to cause frontotemporal dementia and parkinsonism linked to chromosome 17 (FTDP-17). The R406W tau mutation is a unique missense mutation whose patients have been reported to exhibit Alzheimer's disease (AD)-like phenotypes independent of amyloid-beta (Aβ) accumulation, rather than the more typical FTDP-17 phenotypes. The underlying molecular mechanisms of the disease pathogenesis need to be further elucidated, as there are currently no effective treatments available. In this dissertation, patient-derived human iPSC models were established in order to investigate the disease pathology induced by the *MAPT* R406W mutation. iPSCs were generated from FTDP-17 patients harboring the R406W tau mutation and isogenic lines were established using CRISPR/Cas9 to assess genotype-phenotype relationship. The iPSCs were then induced into cerebral organoids, which were dissociated into cortical neurons with high purity. In this neuronal culture, the mutant tau protein exhibited reduced phosphorylation levels at specific epitopes and was increasingly fragmented by calpain. Furthermore, the mutant tau protein was mislocalized and the axons of the patient-derived neurons displayed morphological and functional abnormalities, which were rescued with microtubule stabilization. The findings of the current study provide novel mechanistic insight into tau pathology and a potential for therapeutic intervention.

Introduction

Prevalence of dementia

Dementia is a group of neurodegenerative disorders associated with progressive cognitive impairment. The most common cause of dementia is Alzheimer's disease (AD), which accounts for approximately 70% of all dementia[1]. The major risk factor for AD and other dementias is increasing age, with the majority of patients being 65 or older[2,3]. As the world faces a global trend in population aging, the number of patients is expected to increase substantially—while the estimated number of patients was 46.8 million in 2015, the number is expected to rise to 131.5 million by 2050, which is almost a three-fold increase[4]. This increase will not only have a profound impact on the burden of social and economic costs, but more importantly, the quality of life and lifespan of the affected will be dramatically altered. Records have indicated that the number of deaths caused by AD between 2000 and 2017 has almost doubled, while those caused by other major causes of death including heart disease, cancers, and HIV, have decreased or remained unchanged[3]. Despite the urgent need of treatments for AD and other dementias, none of the treatments currently available can effectively prevent the progression of the disease. Lack of understanding of the molecular mechanisms and biological processes of the disease is one factor contributing to the difficulty in developing novel therapies for dementia.

Alzheimer's disease and the amyloid cascade hypothesis

In 1906, Alois Alzheimer reported the first case of AD and described the histopathological findings that he observed in the postmortem brain of the patient, which includes the presence of senile plaques and neurofibrillary tangles (NFTs)[5]. The accumulations of these lesions, which are composed of the amyloid-beta (Aβ) protein[6] or hyperphosphorylated tau proteins[7-9], respectively, are now known to be the major pathological hallmarks of AD. AD and dementia researches have focused on these two proteins in order to elucidate their roles in disease pathology. Numerous studies have supported the idea of Aβ deposits as being the most upstream cause of AD. For example, assessment of the temporal changes in AD biomarkers has shown that the levels of Aβ-plaque biomarkers are elevated relatively early in the course of the disease, long before the appearance of clinical symptoms, while those associated with tau-mediated neuronal injury or dysfunction rise later as the symptoms progress[10]. In addition, early-onset familial cases of AD are caused by mutations in the *amyloid beta precursor protein (APP)* [11], *presenilin 1 (PSEN1)*[12], and *presenilin 2 (PSEN2)*[13] genes, which are all involved in Aβ production. These findings are in support of the "amyloid cascade hypothesis," which proposes that the aggregation and deposition of the Aβ protein is the cause of further downstream AD pathology, including tau pathology and NFT accumulation, neuronal dysfunction and loss, and finally dementia[14,15]. Based on this hypothesis, multiple therapeutics targeting Aβ have been tested in clinical trials, but most

have been discontinued due to lack of efficacy[16]. Though these repeated failures may be partially attributed to invalid endpoints and the recruitment of symptomatic participants who are at the advanced stage of the disease and are unlikely to benefit from the tested treatments, the validity of the amyloid cascade hypothesis is questionable and alternative therapeutic strategies are currently being taken into consideration.

Tau and FTDP-17 R406W mutation

Another major alternative approach currently undergoing for dementia therapeutics is targeting the tau protein. One rationale for targeting tau is because NFT load, but not amyloid load, correlates with the severity of dementia and neuronal loss in the patient's brains[17,18].

Tau is a soluble microtubule-associated protein primarily expressed in the axons of neurons, which functions in assembling and stabilizing microtubules[19,20]. In neurodegenerative disorders with tau pathology, which are referred to as "tauopathies," tau becomes hyperphosphorylated, which supposedly disrupts its binding ability to microtubules and promotes its self-assembly into insoluble aggregates called paired helical filaments (PHFs), which are the precursors of NFTs[8,9,21]. These tau aggregates have been reported to spread from neuron to neuron, which provides a basis for the spatiotemporal development of tau pathology with disease progression[22].

Importantly, mutations in the *microtubule-associated protein tau (MAPT)* gene, which

encodes the tau protein, have been reported to cause frontotemporal dementia and parkinsonism linked to chromosome 17 (FTDP-17), a type of early-onset, familial dementia[23-25]. Over 50 mutations on the *MAPT* gene has been reported to cause FTDP-17 with clinically diverse phenotypes[26,27]. The R406W missense mutation is one such pathological mutation located on exon 13 of the *MAPT* gene[26,28,29]. Interestingly, patients with this mutation have been reported to exhibit AD-like phenotypes independent of Aβ plaque deposition[30,31]; early memory impairment is a primary presenting feature, while the more typical FTDP-17 symptoms, including changes in social behavior and personality, as well as motor symptoms[32], are less predominant or not seen at all[33]. Like AD and other dementias, the cellular and molecular mechanisms underlying the onset and progression of FTDP-17 with the tau R406W mutation remains largely unknown.

Tau mouse models

Elucidating the disease mechanism of dementias including AD and FTDP-17 using appropriate models is crucial for the development of novel therapeutic strategies. To date, the most commonly used models for dementia are transgenic mouse models. The first transgenic tau mouse model was developed by overexpressing the longest isoform of wild-type (WT) tau in neuronal cells[34]. In this model, early phenotypical changes including hyperphosphorylation of tau, mislocalization of tau to the somatodendrites, and formation of pretangle lesions were

observed, but no NFTs were detected and other major phenotypes such as neuronal loss and cognitive impairment were not reported. Tau pathology was accelerated with the introduction of tau mutations into the mouse models. Overexpression of the *MAPT* P301L mutation in the JNPL3 mouse model enabled the formation of NFTs along with gliosis and neuronal loss[35]. An even more aggressive model was developed with the overexpression of P301S mutant tau, in which cortical atrophy, neuroinflammation, and synaptic loss/dysfunction were observed in addition to tau hyperphosphorylation and NFT formation[36]. In addition, immunosuppression using FK506 succeeded in attenuating tau pathology in this model.

As described above, transgenic tau models have succeeded in recapitulating certain aspects of tau pathology and provided numerous insights into the disease pathogenesis. With that said, it is important to consider the drawbacks of the animal model as well. For example, most mouse models rely on the overexpression of tau well beyond the endogenous levels, at times in irrelevant brain regions, for the induction of robust disease phenotypes. In addition, species difference between rodents and humans must be taken into account—thus far, it has been challenging to translate findings from mouse models into clinical trials. Therefore, it remains crucial to develop novel preclinical models that could overcome these challenges and more accurately recapture the disease pathology.

Induced pluripotent stem cells (iPSCs)

In 2006, Dr. Shinya Yamanaka of Kyoto University made a major scientific breakthrough by generating induced pluripotent stem cells (iPSCs) from fibroblasts using multiple reprogramming factors[37,38]. iPSCs are pluripotent stem cells with unlimited growth potential and the capacity to differentiate into any cell type of the three germ layers. Unlike embryonic stem cells (ESCs), which is another type of pluripotent stem cell derived from the inner cell mass of the pre-implantation embryo[39], iPSCs can be derived from somatic cells of any individual, which clears ethical issues and thus, opens the door for their use in regenerative medicine and disease research. Major applications of the iPSC technology include cellular transplantation therapy for diseases such as Parkinson's disease[40,41], spinal cord injury[42], and macular degeneration[43], and *in vitro* disease modeling and drug discovery using patient-matched lines. Using patient-derived iPSCs is particularly important for modeling neural diseases, because of the difficulties of obtaining human neurons from actual patients. The iPSCs provide an infinite source of patient neurons that express endogenous levels of proteins of interest. The use of patient-matched iPSC models could thereby provide novel insight into the molecular mechanisms of the onset and progression of neurological disorders including dementia.

Objective

The objective of this dissertation is to establish a model that recapitulates the disease pathogenesis induced by the tau R406W mutation using iPSCs derived from FTDP-17 patients and to identify the molecular mechanisms that lead to neurodegeneration, as a basis for therapeutic development. For this purpose, iPSC lines were established from FTDP-17 patients heterozygously carrying the tau R406W mutation. Manipulation of the CRISPR/Cas9 (Clustered regularly interspaced short palindromic repeats/CRISPR associated protein 9) gene-editing system enabled the generation of wild-type (WT) iPSC lines with the mutation corrected or homozygous mutant lines. These isogenic panels of iPSCs were induced into a homogenous population of cortical neurons via dissociation of three-dimensional (3D) cerebral organoids. This neuronal platform was then used for the assessment of the biochemical changes of the mutant tau and cellular abnormalities.

Materials and Methods

Generation of iPSCs from the patient blood cells

iPSCs were generated from peripheral blood mononuclear cells (PBMCs) or T cells as previously described[44-46]. Briefly, PBMCs were isolated by centrifugation at 15000 g for 20 minutes at room temperature, using the BD VACUTAINER CPT (BD, Franklin Lakes, NJ, USA). Remaining PBMCs were maintained in T cell medium and cultured as T cells. Episomal vectors pCE-hOCT3/4, pCE-hSK, pCE-hUL, pCE-mP53DD (all 0.63 μg), which express OCT3/4, SOX2 and KLF4, L-MYC and LIN28, and p53 dominant negative mutant, respectively, as well as pCXB-EBNA1 (0.5 μg), which express EBNA1 (AddGene IDs: 41813, 41814, 41855, 41856, 41857) were electroporated into 3×10^6 PBMCs or T cells using a Nucleofector 2b Device (Lonza, Basel, Switzerland, V-024 program) with an Amaxa Human T-cell Nucleofector kit (Lonza) according to the manufacturer's instructions. 2 days after transfection, an equal volume of iPSC medium was added to the culture without aspirating the T cell medium. The medium was completely replaced with iPSC medium 4 days after transfection. Colonies with a human embryonic stem cell (ESC)-like morphology were picked up between 26~33 days after transfection and cultured further for cultivation and evaluation. All experimental procedures for iPSCs derived from patients were approved by the Keio University School of Medicine Ethics Committee (approval no. 20080016).

Cell culture

Blood samples from two patients with the *MAPT* R406W mutation were obtained[33], which were maintained in T cell medium, consisting of KBM502 medium (KOHJIN BIO, Saitama, Japan) supplemented with Dynabeads Human T-Activator CD3/CD28 (Thermo Fisher Scientific, Waltham, MA, USA).

iPSCs were maintained on irradiated mouse embryonic fibroblasts (MEF) or SNL 76/7 feeder cells in iPSC medium, consisting of DMEM/F12 medium (Wako, Osaka, Japan) supplemented with 0.08 mM MEM-Non Essential Amino Acid Solution (MEM-NEAA, Sigma-Aldrich, St. Louis, MO, USA), 2 mM L-glutamine, 20% (v/v) Knockout Serum Replacement (KSR, Thermo Fisher Scientific), 80 U/ml penicillin, 80 µg/µl streptomycin, 0.1 mM 2-mercaptoethanol, and 10 ng/ml basic fibroblast growth factor (bFGF, PeproTech, Rocky Hill, NJ, USA). Feeder-free iPSCs were maintained on culture dishes coated with 0.25~0.5 µg/µl iMatrix-511 (Laminin-511E8) (Wako) in StemFit AK02N medium (Ajinomoto, Tokyo, Japan). Medium was changed every day for iPSCs on feeder and every other day for feeder-free iPSCs.

Generation and dissociation of cerebral organoids

Organoids were generated from the iPSCs as previously described with slight modifications[47,48]. Briefly, on day 0 of organoid culture, iPSCs were dissociated and 3×10^4 cells were aggregated into embryoid bodies (EBs) in low attachment V-shaped 96-well plates

(Sumitomo Bakelite, Tokyo, Japan). For 6 days, the EBs were maintained in StemFit AK02N medium supplemented with 30 μM Y-27632, as well as 5 μM SB431542 and 2.5 μM IWP-2 to specifically induce them into the forebrain region of neural tissue. On day 6, the medium was changed to neural induction medium consisting of 1% (v/v) N2 Supplement (Thermo Fisher Scientific), 1% (v/v) Glutamax (Thermo Fisher Scientific), 1% (v/v) MEM-NEAA, 2.5 μM IWP-2, 5 μg/ml sodium heparan sulfate (Sigma-Aldrich), and 1% (v/v) penicillin/streptomycin in DMEM/Ham`s F-12 medium (Thermo Fisher Scientific). On day 9, the EBs were transferred into Ultra-Low Attachment surface 6 well plates (Corning, Corning, NY, USA), grown in differentiation media composed of a 1:1 mixture of DMEM/Ham`s F-12 medium and Neurobasal medium (Thermo Fisher Scientific), supplied with 1% (v/v) N2 supplement, 2% (v/v) B27 supplement without vitamin A (Thermo Fisher Scientific), 100 μM 2-mercaptoethanol, 2.5 μg/ml insulin (Wako), 1% (v/v) Glutamax, 0.5% (v/v) MEM-NEAA, and 1% (v/v) Matrigel (Corning). The plates containing the EBs were maintained on a shaker to enhance nutrient and oxygen absorption. On day 15, the medium was changed to differentiation medium consisting of B27 supplement with vitamin A (Thermo Fisher Scientific). The medium was changed every 5~7 days from then on.

Day 30 organoids were dissociated into single cells using the Nerve Cell Dissociation Medium A (KAC, Kyoto, Japan). 5×10^4 cells, 1×10^5 cells, and 5×10^5 cells were plated onto 60 μg/ml Poly-L-Ornithine (Sigma-Aldrich) and 10 μg/ml laminin (R&D Systems, Minneapolis,

MN, USA)-coated 96 well, 48 well, and 12 well cell culture plates, respectively (Greiner Bio-One, Kremsmünster, Austria) and cultured for another additional 30 days in Neurobasal medium supplemented with 1% (v/v) B27 supplement with vitamin A, 0.25% (v/v) Glutamax, and 1% (v/v) penicillin/streptomycin.

Pluripotency check of iPSC clones

The iPSC clones were immunostained for pluripotency markers alkaline phosphatase using SIGMAFAST BCIP/NBT (Sigma-Aldrich) according to the manufacturer's instructions, and anti-TRA-1-60 (mouse, 1:500 dilution, EMD Millipore, Billerica, MA, USA).

Karyotype analysis

G-banding analysis of the iPSC lines was conducted by the LSI Medience Corporation (Tokyo, Japan).

Construction of targeting vectors and Cas9 vector

The *MAPT* locus containing exon 13 with or without the R406W mutation was cloned from the patient genome into the pCR-Blunt II-TOPO vector (Thermo Fisher Scientific) by PCR using the following primers: forward TTTTTGGCTTTACCAGATGCTCA, reverse TCATTACTGAGAAGGGGTGGTGA. The PCR conditions are as follows: 35 cycles of 98℃

for 10s, followed by 68℃ for 3 min 30s. The PrimeSTAR Max DNA Polymerase (Takara, Kusatsu, Japan) was used. A 2-kb 5′arm and 5-kb 3′arm consisting of exon 13 with the mutation site were cloned individually into separate entry vectors by PCR using the following primers: 5′arm forward, AACTTTGTATAATAAAGTTGTGACTGAGTGGGTCTGGATAGG, 5′arm reverse, CAGACTATCTTTCTAGGGTTAAGTTTCTTGTGTACCCTCCAG, 3′arm forward, ATGATTATCTTTCTAGGGTTAAAATGATCACTGTCTCTGGGG, 3′arm reverse, CAACTTTGTATAGAAAAGTTGCTAAGGGTGCGTGGGAAAGA. The PCR conditions are as follows: 98℃ for 1 min, followed by 20 cycles of 98℃ for 10s and 68℃ for 2 min (5′arm) or 5 min (3′arm). Using the GeneArt Seamless Cloning and Assembly Kit (Thermo Fisher Scientific), these entry vectors, along with another entry vector consisting of a selection cassette with Puromycin-ΔTK driven by a mouse PGK promoter and PiggyBac inverse terminal repeats (ITRs) at both ends, were assembled into a single destination vector.

The Cas9 expression plasmid vector pSPCas9(BB)-2A-Puro (PX459) was obtained from AddGene (ID: 48139). Complementary oligonucleotides encoding sgRNA were annealed and cloned into the *Bbs*I site in the Cas9 vector. The sequences of the oligonucleotides are as follows: upper, CTTAAAATGATCACTGTCTCTGG, lower, AAACGAGACAGTGATCATTTTAAGC.

Transfection of targeting vector into iPSCs

Feeder-free iPSCs were pre-treated with 10 μM Y-27632 (EMD Millipore) overnight to prevent apoptosis induced by dissociation[49]. The iPSCs were dissociated into single cells with Tryple Select (Thermo Fisher Scientific). The targeting vector with or without the R406W mutation and the Cas9 expression vector were electroporated into 1×10^6 iPSCs using NEPA21 (NepaGene, Chiba, Japan). Transfected cells were plated onto iMatrix-511-coated 60 mm dishes (Iwaki, Chiba, Japan). Y-27632 was removed from the culture 2 days after the transfection. Cells were treated with 0.75~0.8 μg/μl puromycin on days 2, 3, 6, and 8 after plating.

Colonies with a human ESC-like morphology were picked up and DNA from each colony was extracted using the DNeasy Blood & Tissue Kit (QIAGEN, Hilden, Germany). PCR analysis evaluating the knock-in of targeting vectors was performed using the following primers: forward, GCGTCCCAGAAAGGGTATAGG, reverse GTCACGTAAAAGAATTGTTTGTTGA. The DNA of the clones in which knock-in occurred was analyzed by Sanger sequencing with the 3130xl Genetic Analyzer (Applied Biosystems, Waltham, MA, USA) to check the mutation site.

Excision of PiggyBac cassette from iPSCs

Feeder-free iPSCs pre-treated with 10 μM Y-27632 overnight were dissociated into single cells with Tryple Select (Thermo Fisher Scientifc). 1 μg PBx (Excision Only PiggyBac

Transposase; Funakoshi, Tokyo, Japan) was transfected into 1×10^6 iPSCs with the GeneJuice Transfection Reagent (EMD Millipore) and plated onto iMatrix-511-coated 10 cm dishes (Iwaki). DNA extraction and PCR analysis were performed as described above.

Immunofluorescence

The cells were fixed in 4% (w/v) paraformaldehyde for 15~20 min at room temperature, followed by washing in phosphate buffer saline (PBS) three times for 5 min each. After permeabilization with 0.2% (v/v) Triton X-100 for 15~20 min, the cells were again washed in PBS three times for 5 min each. Samples were incubated in StartingBlock (TBS) Blocking Buffer (Thermo Fisher Scientific) for 1 hour at room temperature. Incubation with primary antibodies was performed overnight at 4℃. The following primary antibodies and dilutions were used: anti-TBR1 (rabbit, Abcam, Cambridge, UK, ab31940, 1:200 dilution), anti-MAP2 (chicken, Abcam ab5392, 1:10000 dilution), anti-βIII-tubulin (rabbit, Abcam, ab18207, 1:1000 dilution), anti-FOXG1 (rabbit, Abcam, ab18259, 1:500), and anti-tau (RTM38, Fujifilm Wako Pure Chemical, Osaka, Japan; rat, 1:5000 dilution). The following day, the cells were incubated with secondary antibodies for 1 hour at room temperature. Secondary antibodies used include Goat Alexa 488, 555, and 647 conjugates (Thermo Fisher Scientific, 1:500 dilution). Nuclear staining was performed with the Cellstain DAPI solution (DOJINDO, Kumamoto, Japan, 1:1000 dilution) for 15~20 minutes at room temperature.

The following day, the cells were incubated with secondary antibodies for 1 hour at room temperature. The cells were observed with a Zeiss LSM700 confocal microscopy. The quantification of the immunofluorescence was performed with In Cell Analyzer 6000 (GE Healthcare, Little Chalfont, UK).

Western blot

Cells were dissociated from the culture plates and dissolved in lysis buffer containing 20 mM HEPES, 1 mM $MgCl_2$, 100 mM NaCl, 0.5 % NP-40, 1 mM dithiothreitol (DTT), 0.4 mM Pefabloc (AEBSF), 10 μg/ml leupeptin, 10 mM NaF, and 10 mM β-glycerophosphate. After homogenization and sonication, the samples were centrifuged at 15,000 x g for 15 min at 4℃. For dephosphorylation, samples were treated with 20 U Lambda Protein Phosphatase (New England Biolabs, Ipswich, MA, USA) for 3 hours at 30℃. The protein samples were diluted in 4x Laemmli Buffer (BioRad, Hercules, CA, USA) with 10 mM 2-mercaptoethanol and boiled at 95℃ for 5 min. The lysates and the Tau Protein Ladder (rPeptide, Athens, GA, USA) were loaded onto Extra PAGE One Precast Gels 7.5-12.5% (NACALI TESQUE). SDS-polyacrylamide gel electrophoresis (PAGE) was performed at 120V for 105 min. The proteins separated in the gel were transferred onto an Immobilon-P membrane (EMD Millipore). The membranes were blocked with 5 % (w/v) skim milk for 30 min and incubated with antibodies diluted in Can Get Signal Immunoreaction Enhancer Solutions (TOYOBO, Osaka, Japan). The

following primary antibodies were used: anti-tau (K9JA) (Agilent Technologies, Santa Clara, CA, USA, 1:10000 dilution), Tau5 (mouse, 1:2000 dilution), Tau12 (mouse, 1:10000 dilution), Tau46 (mouse, Cell Signaling Technology, Beverly, MA, USA, 4019, 1:2000 dilution), anti-Tau-pT181 (rat, Cell Engineering Corporation, Osaka, Japan, 1:1000 dilution), anti-Tau-pS409 (rabbit, 1:1000 dilution)[50], anti-β-Catenin (rabbit, Cell Signaling Technology, 8480, 1:2000 dilution), anti-p-β-Catenin (S33/S37/T41) (rabbit, Cell Signaling Technology, 9561, 1:1000 dilution), and anti-GAPDH (rabbit, Sigma-Aldrich, G9545, 1:10000 dilution).Signals on the membranes were visualized with the ECL Prime detection kit (GE Healthcare) and the images were acquired on an ImageQuant LAS 4000 (GE Healthcare).

For protease inhibition, dissociated neurons were pre-treated with either 120 μM Z-VAD-FMK (Peptide Institute, Osaka, Japan), pan-caspase inhibitor, or 250 μM ALLN (Nacalai Tesque), pan-calpain inhibitor, for 24 hours before cell lysis.

For quantification, we have normalized levels of phosphorylated tau and tau fragments to total tau and full-length tau, respectively (see corresponding figure legends for further detail). We have not included the quantification of total tau levels in our study because normalization with the highly variable GAPDH levels among different neuronal lines confounded our results.

Phosphorylation analysis of tau

Human Tau cDNAs (0N3R, WT and R406W) were synthesized, and subcloned into

pEGFP-c1 mammalian expression vector. The C-terminus of Tau (308-351 aa; VVSGDTSP(R/W)HLSNVSSTGSIDMVDSPQLATLADEVSASLAKQGL) was subcloned into pGEX-2T E. coli expression vector. GST-PKACa (#01-127) and GST-GSK3β (#04-141) were purchased from Carna Biosciences (Kobe, Japan). GST-Rho-kinase-cat, GST-CDK5, and GST-p35 were expressed in Sf9 cells using a baculovirus system and purified using glutathione Sepharose beads[51].

For *in vitro* analysis, GST-Tau-C (1 μM) was incubated with each kinase (30 nM) in a reaction mixture (25 mM Tris-HCl at pH 7.5, 1 mM EDTA, 1 mM DTT, 5 mM $MgCl_2$, and 50 μM ATP) for 30 min at 30°C. The reaction mixtures were boiled in SDS sample buffer and subjected to western blot analysis.

Plasmids encoding Tau and each kinase were transfected into COS7 cells using the Lipofectamine® 2000 reagent (Thermo Fisher Scientific) according to the manufacturer's protocol. The cells were lysed with SDS sample buffer and subjected to western blot analyses.

Tau localization assay

The localization of tau was analyzed with In Cell Analyzer 6000 (GE Healthcare). Dissociated neurons were immunostained with MAP2, βIII-tubulin, and tau and the percentage of tau on MAP2- and βIII-tubulin-positive regions were quantified. Dendritic and axonal tau were defined as tau on MAP2-positive area, and tau on βIII-tubulin-positive but MAP2-

negative area, respectively.

Neurite puncta count

Confocal images of the neurites were obtained with the Zeiss LSM700 oil immersion 100x objective. The number of puncta on neurites were counted manually. For normalization, the length of the neurites was measured using the Fiji plugin Simple Neurite Tracer. Cultures were treated with or without 20 nM Epothilone D (EpoD; Abcam) for 24 hours for the rescue experiment.

Mitochondria count

In order to visualize mitochondria, the dissociated neurons were transfected with pcDNA3 Mito-eYFP (kindly provided by Drs. T. Tomiyama and T. Umeda, Osaka City University) and tdTomato expression vectors. Confocal images of the mitochondria on the axons were taken with the Zeiss LSM700 oil immersion 63x objective. The numbers of mitochondria were counted manually. For normalization, the length of the neurites was measured using the Fiji plugin Simple Neurite Tracer.

Live imaging mitochondrial trafficking

Transfected neurons were visualized with the Olympus FV3000 Confocal Laser

Scanning Microscope with a silicon-oil immersion 63x objective. 1.6x~2.0x digital zoom was used for better viewing. Images were taken at 5-second intervals for a total of 100 frames.

Statistical analysis

All data from at least three independent experiments are expressed as means ± SEM. All replicates are from different batches of organoids that have been dissociated in separate experiments. GraphPad Prism 8 was used for statistical analysis. The normality of data was assessed using the Shapiro-Wilk test and variances were compared using the Brown-Forsythe test. Data were analyzed with the unpaired, two-tailed Student`s t-test and one- or two-way ANOVA followed by Tukey-Kramer`s multiple comparisons test, as indicated in the figure legends. Differences were considered significant when $p<0.05$.

List of plasmids used in this study

Plasmid name	Features
pSPCas9(BB)-2A-Puro (PX459)	Mammalian expression vector, CBh promoter, Cas9
pGEX-2T-Tau-C-WT/R406W	E.coli expression vector, tac promoter, GST-Tau-C (human 0N3R, 308-351 aa)
pEGFP-c1-Tau-WT/R406W	Mammalian expression vector, CMV promoter, EGFP-Tau (human 0N3R, 1-351 aa)
pCGN-HA-GSK3B-CA	Mammalian expression vector, CMV promoter, HA-GSK3B-CA (human)
pEF-BOS-GST-PKA-CA	Mammalian expression vector, EF-1α promoter, GST-PKA-CA (mouse)
pEF-BOS-GST-Rho-	Mammalian expression vector, EF-1α promoter, GST-Rho-

kinase-cat	kinase catalytic region (bovine)
pEF-BOS-GST-CDK5	Mammalian expression vector, EF-1α promoter, GST-CDK5 (human)
pEF-BOS-GST-p35	Mammalian expression vector, EF-1α promoter, GST-p35 (human)
pcDNA3-Mito-eYFP	Mammalian expression vector, CMV promoter, Mito-eYFP
ptdTomato	Mammalian expression vector, CMV promoter, tdTomato

Results

Generation and characterization of the *MAPT* R406W iPSCs

MAPT R406W iPSCs were established from 2 Japanese FTDP-17 patients (Patients #1 and #2) of the same pedigree, who were both heterozygous for the mutation and exhibited memory impairment as their primary symptom[33] (Table 1). DNA sequencing confirmed that the patients were heterozygous for the mutation (*MAPT* $^{R406W/+}$, Fig. 1). The patients had no other mutations besides the *MAPT* R406W mutation, as previously confirmed by DNA sequencing of the *APP, PSEN1*, *PSEN2*, and *PRGN* genes, which are the major genetic causes of familial AD and FTDP-17[33].

The iPSCs were generated using the integration-free episomal vector system, as described previously[44-46]. Episomal vectors harboring multiple reprogramming factors were electroporated into the patients' PBMCs and T-cells (Fig. 2A). 40 clones derived from patient #1 and 30 clones derived from patient #2 were picked up and expanded. Because some clones were lost during expansion, a final number of 11 clones from patient #1 (passage 5 or 6) and 16 clones from patient #2 (passage 4) were obtained. PCR analysis confirmed the removal of the episomal vectors from 9 out of 11 clones for patient #1 and 5 out of 16 clones for patient #2 (Fig. 2B). Several integration-free clones from each patient were characterized by pluripotency staining and karyotyping (Fig. 3). These clones stained positively for pluripotency markers alkaline phosphatase (AP) (Fig. 3A) and TRA-1-60 (Fig. 3B) and were karyotypically

Table 1. iPSC donor information

	Patient #1*	Patient #2*	Patient #3†
Gender	Female	Male	Female
Age at onset	50	47	N/A
Age at examination	67	48	N/A
Age at biopsy	N/A	N/A	70
Origin	Peripheral mononuclear blood cell	Peripheral mononuclear blood cell	Fibroblast
Reprogramming method	Episomal	Episomal	Sendai virus
Gene-editing	WT, homo	WT, homo	WT

N/A=not available, WT=wild-type, homo=homozygous

*Modified from Ikeuchi et al., 2011

†Reference 52

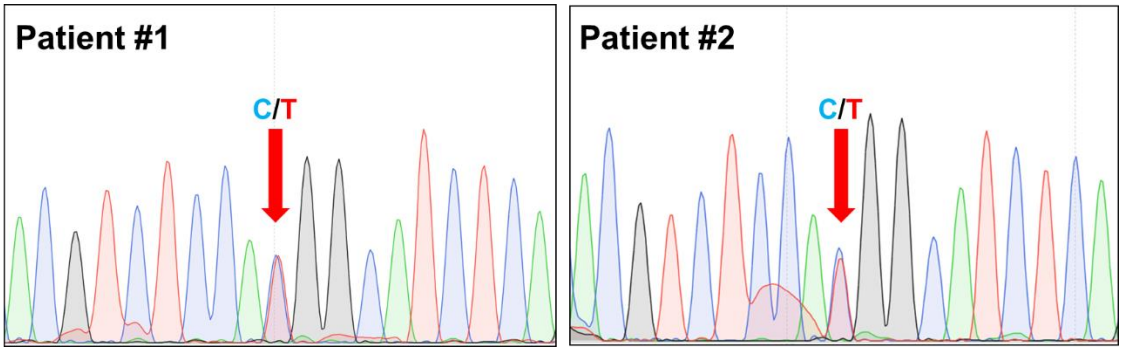

Figure 1. DNA sequence analysis for the *MAPT* R406W mutation in FTDP-17 patients. Sanger sequencing of DNA obtained from peripheral mononuclear blood cells of the FTDP-17 patients (Patients #1 and #2; see Table 1) confirmed that the patients were heterozygous for the *MAPT* R406W mutation (NM_005910.5: c.1216C>T).

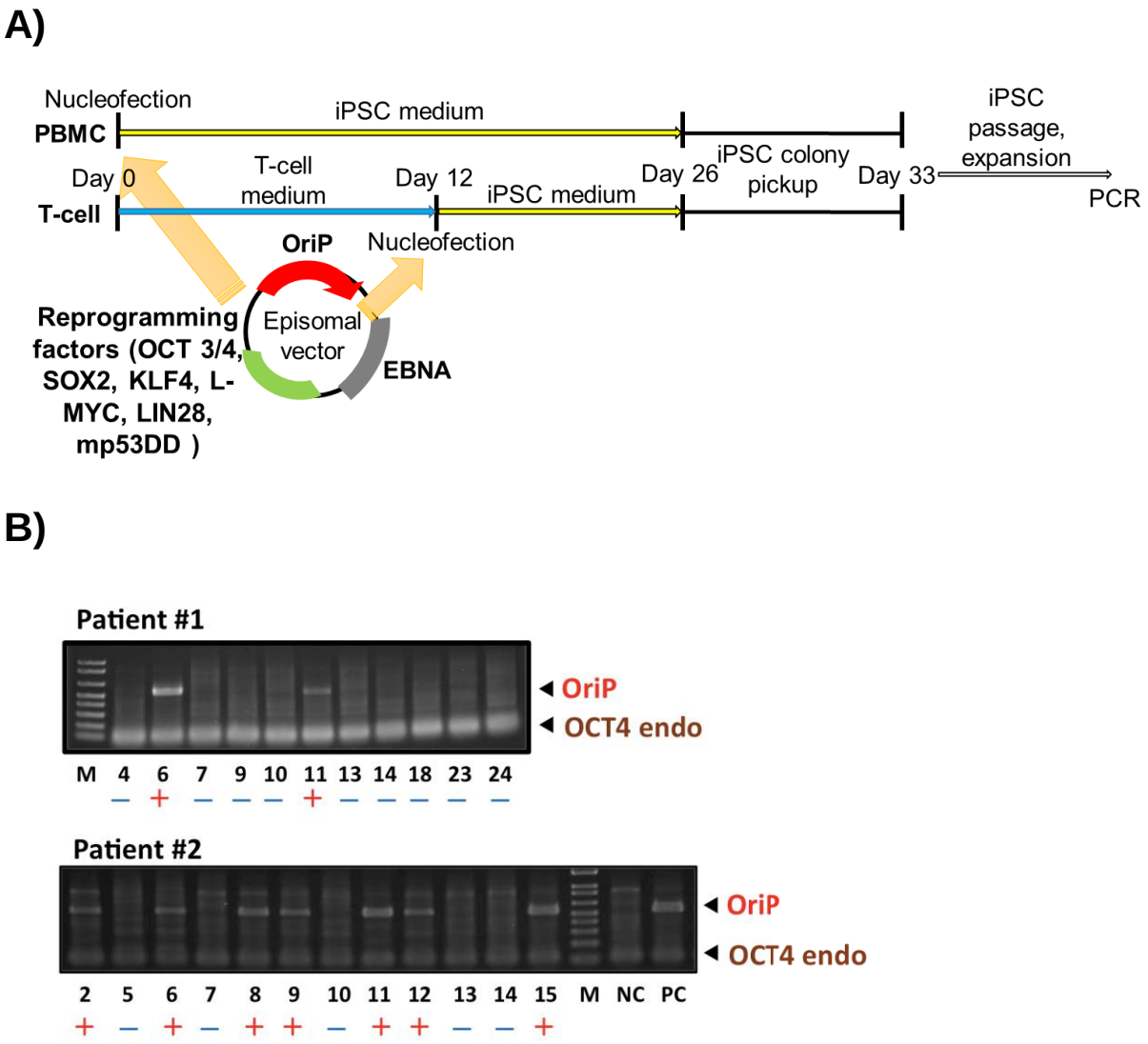

Figure 2. Generation of *MAPT* R406W iPSCs using episomal vectors.

(A) Schematic of the reprogramming method. Episomal vectors harboring reprogramming factors (OCT3/4, SOX2. KLF4, L-MYC, LIN28, and mp53DD) were electroporated into the FTDP-17 patients' PBMCs or T-cells. The cells were then cultured in standard iPSC medium, until the appearance of ESC-like colonies. Between Days 26~33, iPSC colonies were picked up and expanded for subsequent analysis.

(B) PCR analysis for residual episomal vectors. iPSC clones without the episomal OriP sequence is considered integration-free (NC=negative control, PC=positive control).

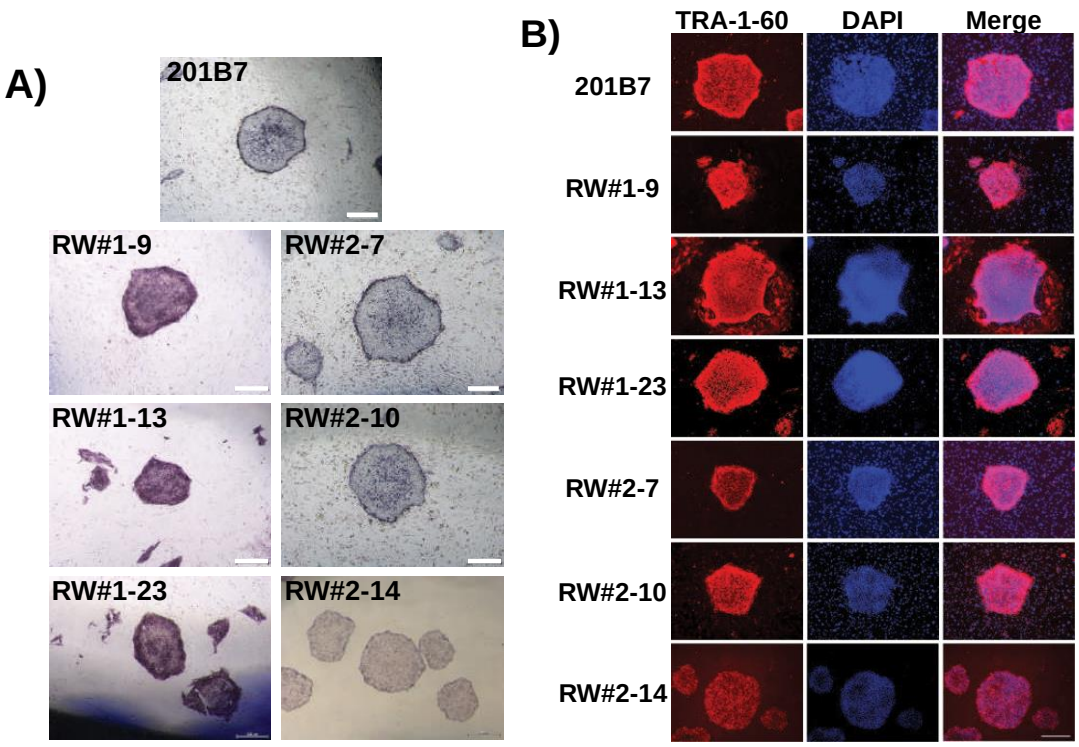

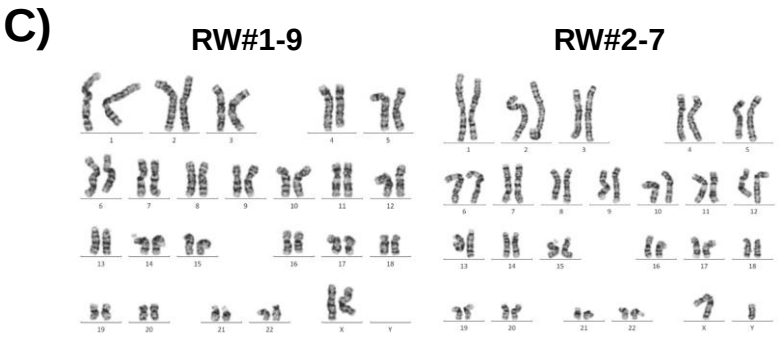

Figure 3. Characterization of the *MAPT* R406W iPSC clones.

(A~B) Immunofluoresence of the *MAPT* R406W iPSC clones with pluripotency markers alkaline phosphatase (A) and TRA-1-60 (B). Scale bar=500 μm.

(C) Karyotyping of representative iPSC clones.

normal (Figure 3C).

Another *MAPT* R406W iPSC line generated with Sendai virus vectors from a symptomatic subject of an unrelated pedigree (Patient #3; Table 1), who was also heterozygous for the mutation[52], will be used for the subsequent studies. In addition, the 201B7 iPSC line, derived from a healthy subject, was obtained for use as a control[38].

Generation of isogenic iPSC lines with CRISPR/Cas9

Next, the CRISPR/Cas9 technology was utilized to generate panels of isogenic iPSC lines[53], in order to reduce the variability of experiments caused by genetic heterogeneity and to assess genotype-phenotype relationship. Targeting vectors were designed to include exon 13 of the *MAPT* locus either with or without the R406W mutation on the 3' arm, for inducing the mutation into the wild-type (WT) allele or for correcting the mutation, respectively (Fig. 4A). In addition, a puromycin selection cassette was placed in between the two arms with PiggyBac inverted terminal repeats (ITRs) at both ends (Fig. 4A). Transfection experiments were performed and colonies that survived puromycin selection were picked up and analyzed. Consequently, DNA sequencing revealed the successful manipulation of the mutation site, confirming the generation of isogenic wild-type (WT: $MAPT^{+/+}$) lines and homozygous mutant ($MAPT^{R406W/R406W}$) lines (Fig. 4B). Finally, the gene-edited clones were transfected with the PiggyBac transposase for excision of the selection cassette[46]. The PiggyBac transposase recognizes the PiggyBac ITRs at the ends of the selection cassette and removes the cassette

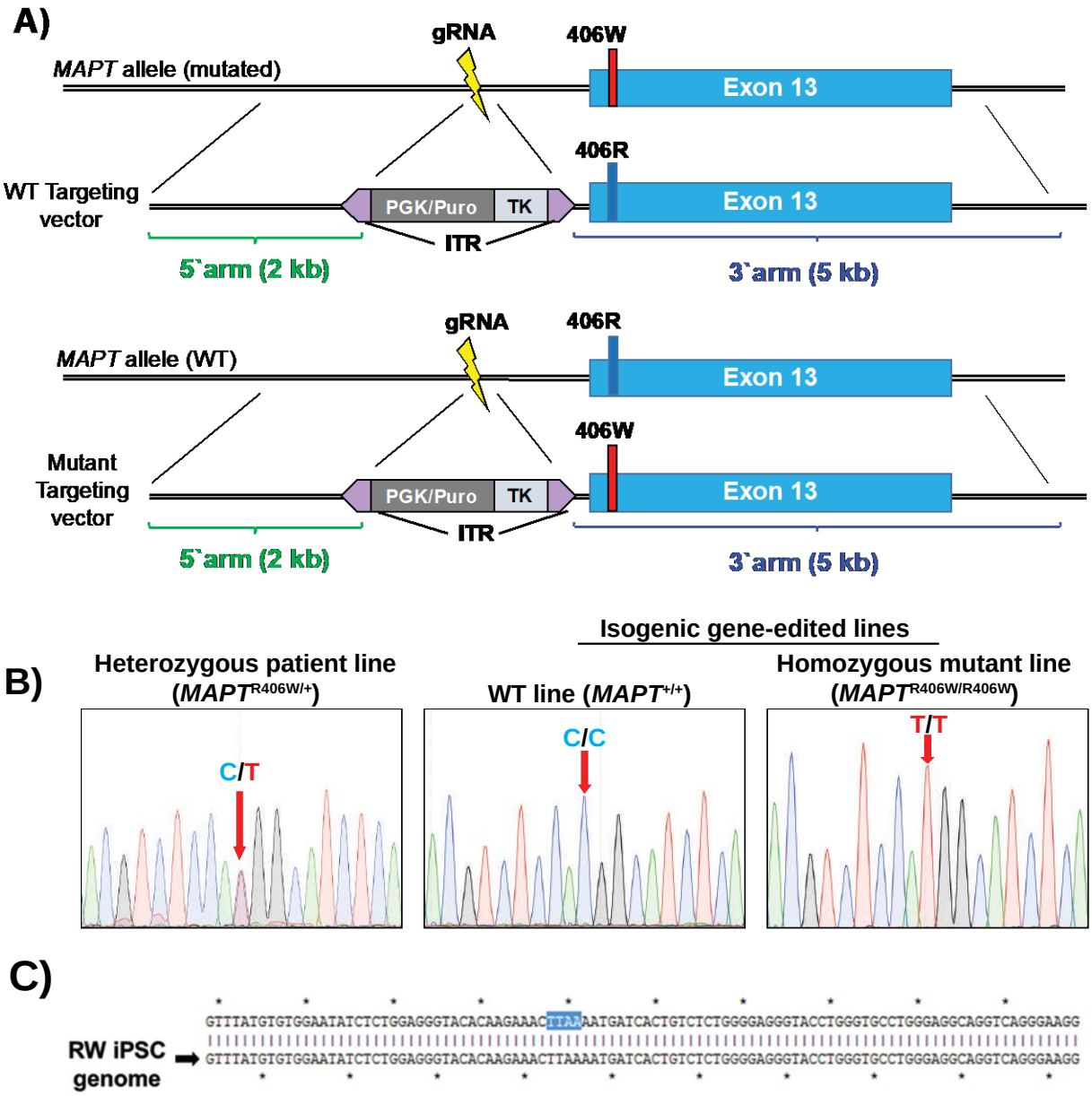

Figure 4. Gene-editing of *MAPT* R406W iPSCs using CRISPR/Cas9.

(A) Schematic of the targeting vectors intended to correct the R406W mutation (top; WT targeting vector) or induce the R406W mutation into the wild-type (WT) *MAPT* allele (bottom; mutant targeting vector).

(B) Sanger DNA sequencing of an original heterozygous FTDP-17 iPSC line (left; $MAPT^{R406W/+}$) and the isogenic gene-edited iPSC lines—WT lines (middle; $MAPT^{+/+}$) and homozygous mutant lines (right; $MAPT^{R406W/R406W}$).

(C) DNA sequence of a representative gene-edited iPSC clone after excision of the selection cassette. The genomic TTAA sequence is left intact and there are no unintended indels or mutations.

inserted in between the TTAA sequence of the genome without leaving any trace behind, thus enabling the generation of a "footprint-free" gene-edited iPSC clone. DNA sequence analysis of the manipulated region indeed confirmed that these isogenic clones were free of genomic indels and other unintended mutations (Fig. 4C).

Establishment of iPSC-derived neuron-rich culture via dissociation of cerebral organoids

The iPSC lines were then subjected to neuronal differentiation for subsequent analysis (Fig. 5). We utilized the method for inducing cerebral brain organoids[47,48], which are three-dimensional (3D) spheres that mimic human brain development and environment, including layer-like structures, regionality, and heterogenous composition of cells. Previous reports have implicated that because of their similarity to actual brains, disease pathology may be accelerated in organoids compared to conventional 2D cultures[54]. However, because cerebral organoids consist of a heterogenous population of cells[55] and the cells within the organoids are densely packed, the usage of cerebral organoids as a whole was not suitable for biochemical analyses of tau and morphological observations of neurons. Thus, a novel method was devised to isolate a pure population of cortical neurons from the organoids. After 30 days of culture, at which point the presence of neuronal cells has been identified within the organoids (data not shown), the organoids were dissociated using a papain-based solution and single neurons were plated onto typical 2D culture dishes. Because the neurites were trimmed off due to enzymatic

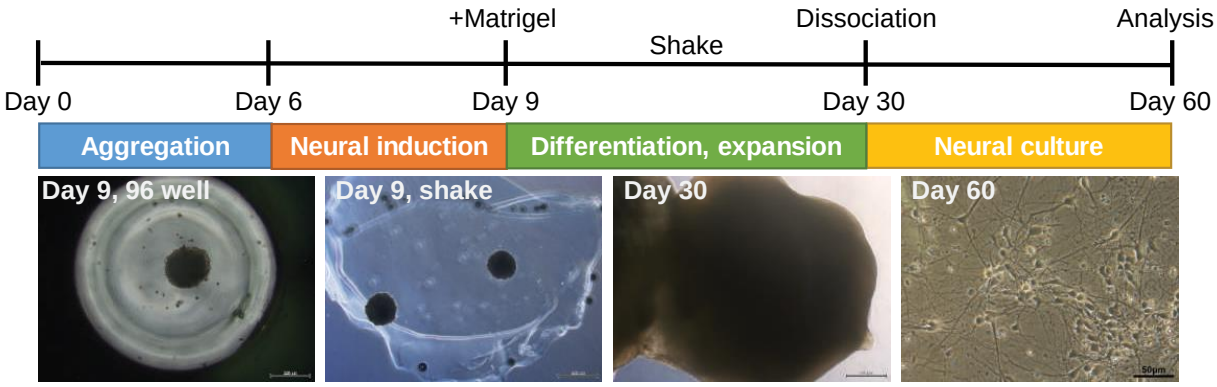

Figure 5. Neuronal differentiation of iPSCs via dissociation of cerebral organoids

Schematic timeline for neuronal differentiation of iPSCs using the protocol for cerebral organoid induction. Organoids were dissociated into cortical neurons and cultured on typical two-dimensional plates. All analyses were performed after a total of 60 days of culture. Scale bar=500μm (Day 9 and Day 30), 50μm (Day 60).

processing, the dissociated neurons were further cultured to enable the re-growth of the neurites and polarization of the axons and dendrites. Using brightfield observation, the majority of the neurons were deemed to have developed multiple neuritic processes and polarity by 30 days post dissociation. At this timepoint, these cultures were subjected to immunofluorescence to evalulate the expression of neuronal markers. Lines that were successfully induced into organoids and dissociated consisted of neurons positive for MAP2, TBR1, and tau (Fig. 6A). Quantification revealed that all the lines evaluated were >85% positive for neuronal markers MAP2 and β-III tubulin (Figs. 6B and 6C), and also highly positive for forebrain (cortical neuron) markers TBR1 and FOXG1, as well as NEUN, indicating the presence of mature neurons (Figs. 6D-6F), with similar differentiation efficiency among lines.

Unfortunately, because all the iPSC lines derived from Patient #1 did not efficiently differentiate into neurons with our protocol, iPSC-derived neurons derived from Patient #2 and #3 were utilized for subsequent analysis. Majority of the experiments were done with iPSC lines from Patient #2, because both *MAPT* $^{+/+}$ and *MAPT* $^{R406W/R406W}$ lines have been generated from this patient and they all stably differentiated into neurons with the current protocol. iPSC lines from Patient #3 were mainly utilized to reconfirm the results obtained with those from Patient #2.

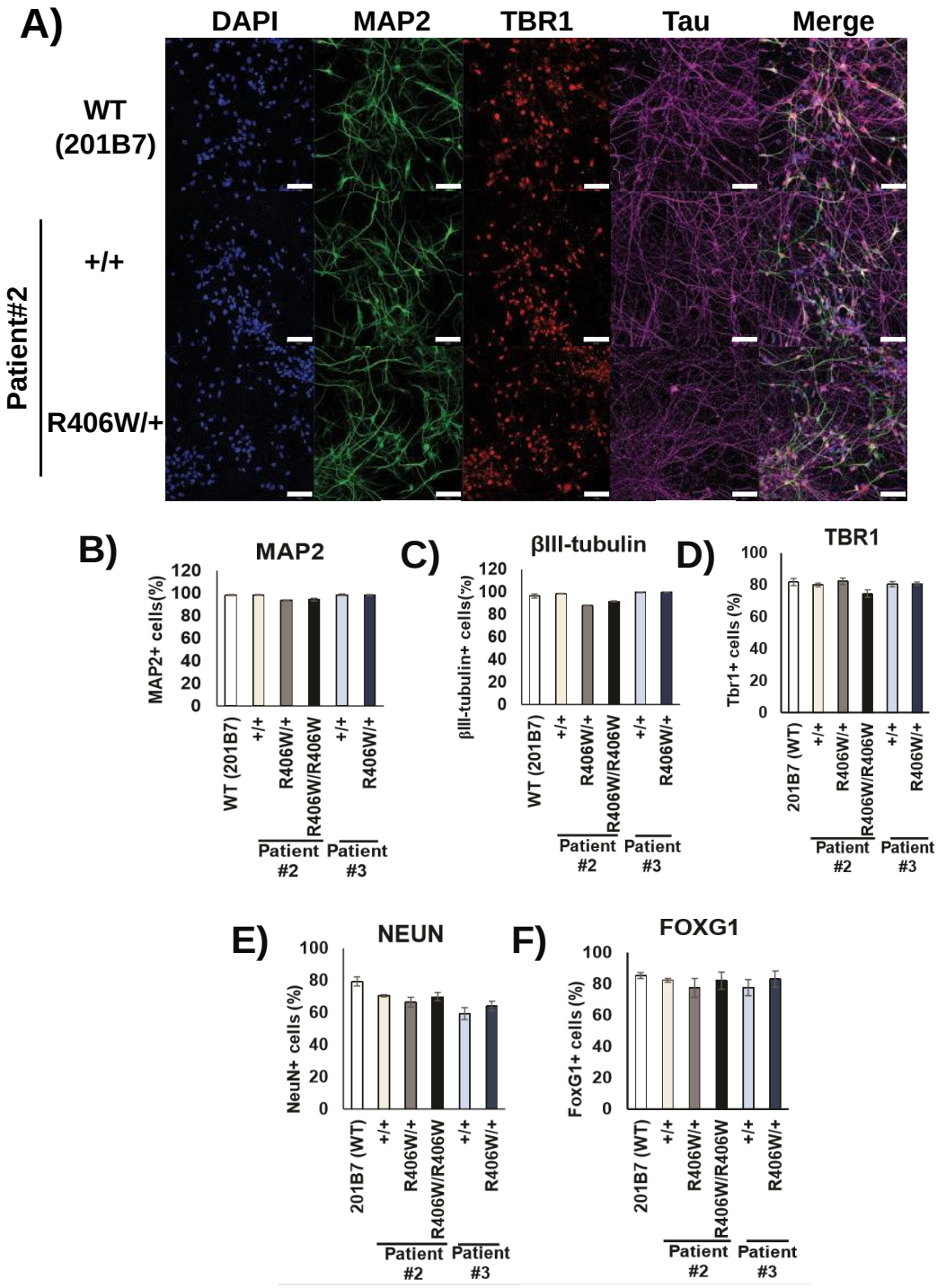

Figure 6. Characterization of iPSC-derived neurons.

(A) Immuofluorescence of iPSC-derived neurons with neuronal marker MAP2, cortical neuron marker TBR1, and tau. Scale bar=50 μm.

(B-F) Quantification of the percentage of cells positive for neuronal markers (MAP2, B; βIII-tubulin, C; NEUN, E) and forebrain markers (TBR1, D; FOXG1, F) (n=3).

R406W mutant tau is less phosphorylated by multiple kinases

Abnormal tau hyperphosphorylation is a key hallmark of tauopathies[9,21]. Thus, changes in tau phosphorylation levels and patterns were first investigated in the iPSC-derived neurons. Interestingly, western blot analysis revealed that tau phosphorylation at S409 and T181 were lowered in both *MAPT* $^{R406W/+}$ and *MAPT* $^{R406W/R406W}$ neurons compared to the control neurons 30 days after dissociation (Figs. 7A-7F). The phosphorylation level of S404 also appeared to decrease when analyzed with a S404 phosphorylation-dependent tau antibody (Figs. 7G and 7H), as previously reported[56]. However, reduced phosphorylation was not observed with the PHF1 antibody, which recognizes both S396 and S404 (data not shown), suggesting that the reduction seen with the S404 phosphorylation-specific antibody may simply be reflecting a change in immunogenicity due to the mutation.

Furthermore, co-expression of the GST-conjugated C-terminus fragment of WT or R406W tau with various kinases *in vitro* revealed that the mutation impaired the phosphorylation of S404 by GSK3β and CDK5 and the phosphorylation of S409 by Rho-associated protein kinase (RhoK) and protein kinase A (PKA) (Fig. 8). These findings support the results obtained with the iPSC-derived neurons and suggest that the R406W mutation potentially impairs the phosphorylation of tau by multiple kinases.

In addition, when blotting with pan-tau antibody Tau5, we found that the samples exhibited two major bands (48kD and 55kD). The intensity of the 48kD band was increased in

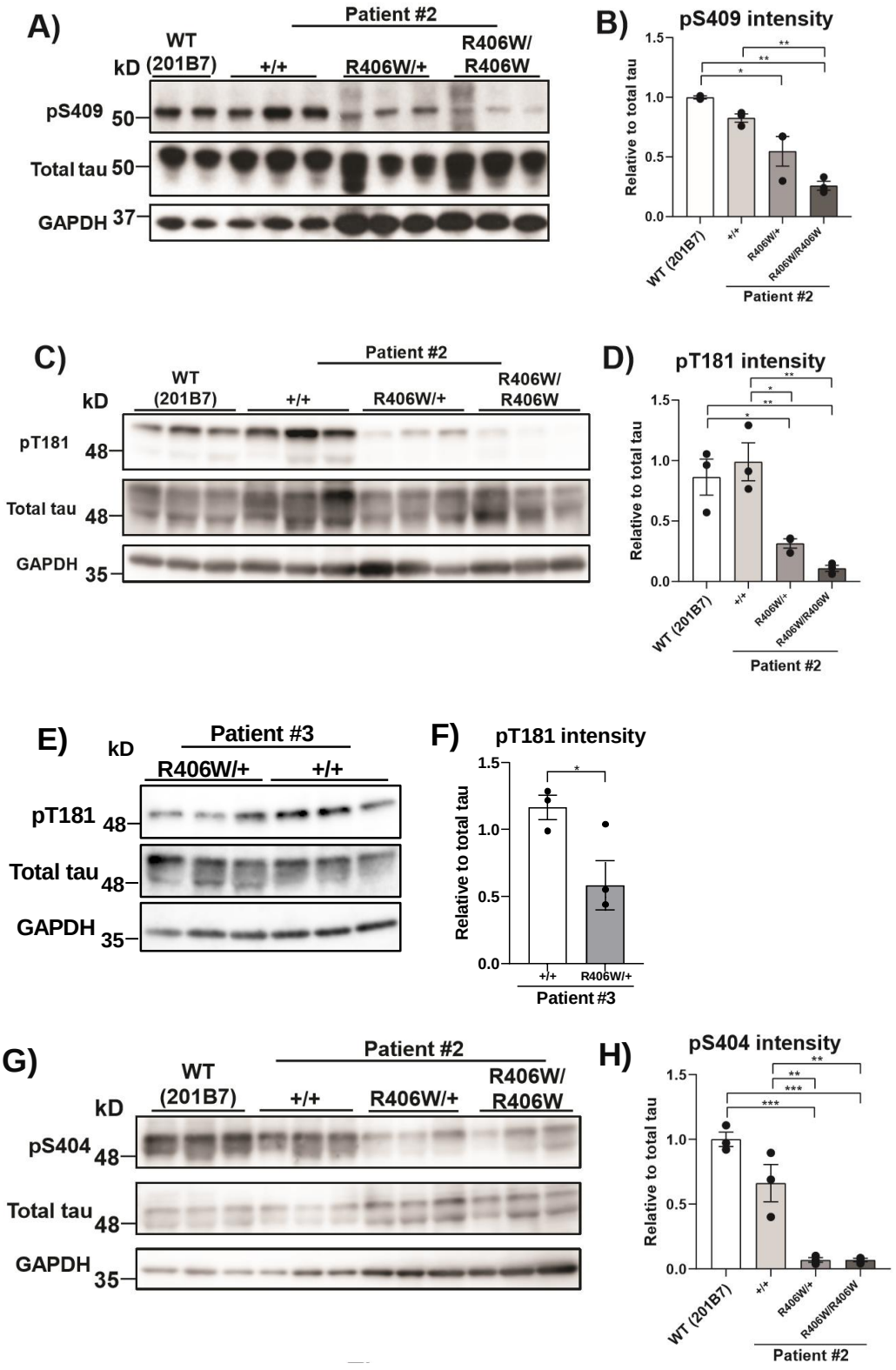

Figure 7. Identification of tau epitopes with reduced phosphorylation in the mutant neurons.

Western blot analyses using site-specific phosphorylation-dependent tau antibodies revealed decreased phosphorylation levels at S409 (A, B), T181 (C-F), and S404 (G-H) in the $MAPT^{R406W/+}$ and $MAPT^{R406W/R406W}$ neurons (n=3; *p<0.05, **p<0.01, ***p<0.001).

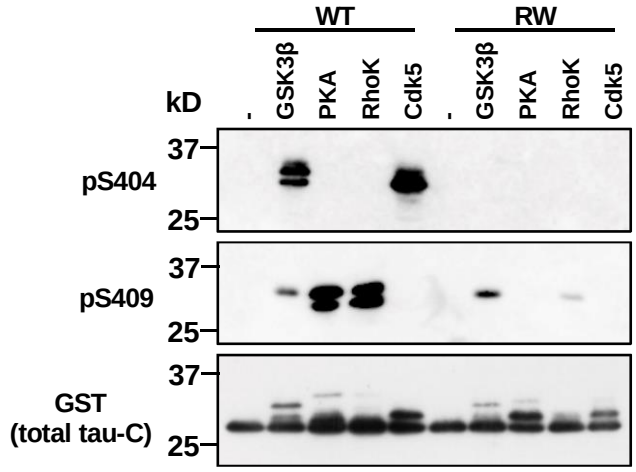

Figure 8. R406W mutation impairs tau phosphorylation by multiple kinases.

Western blot analysis of the C-terminus fragment of WT and R406W (RW) tau after incubation with each respective kinase. In WT tau, S404 was directly phosphorylated by GSK3β and Cdk5, whereas S409 was directly phosphorylated by PKA and Rho-kinase (RhoK), both of which were impaired by the R406W mutation. GSK3β weakly phosphorylated WT and RW tau at S409 to a similar extent.

the mutant samples derived from both Patients #2 and #3 at 30 days after dissociation (Figs. 9A~9D). The two bands differed in the phosphorylation level of tau, with the 48kD band representing the less phosphorylated form of tau (termed “hypophosphorylated” tau from hereon), since both bands shifted downwards and merged into one band representing the 0N3R tau isoform when the samples were treated with λ-phosphatase for dephosphorylation (Figure 9E). Furthermore, the amount of 48kD tau increased with GSK3β inhibition using SB216763, which implicates that GSK3β was the kinase most responsible for the reduced phosphorylation levels of R406W mutant tau (Figs. 10A and 10B). In support of our finding, treatment with CHIR99021, a more specific GSK3β inhibitor, resulted in a dose dependent increase of the 48kD band (Figs. 10C and 10D). This is consistent with the results obtained when co-expressing tau and various kinases in COS-7 cells, showing that S404 and S409 are also potential phosphorylation sites of GSK3β and that their phosphorylation by GSK3β is impaired with the R406W mutation (Figs. 11A~11C). Importantly, the phosphorylation level of β-catenin, another major GSK3β substrate, remained unchanged, implicating that the reduced tau phosphorylation was not due to a change in GSK3β activity, but rather, a change in accessibility to the tau protein because of the mutation (Fig. 12A and 12B).

Collectively, our analyses suggest that the R406W mutant tau was less phosphorylated by multiple kinases, with poor phosphorylation by GSK3β particularly accounting for the overall reduction of phosphorylation.

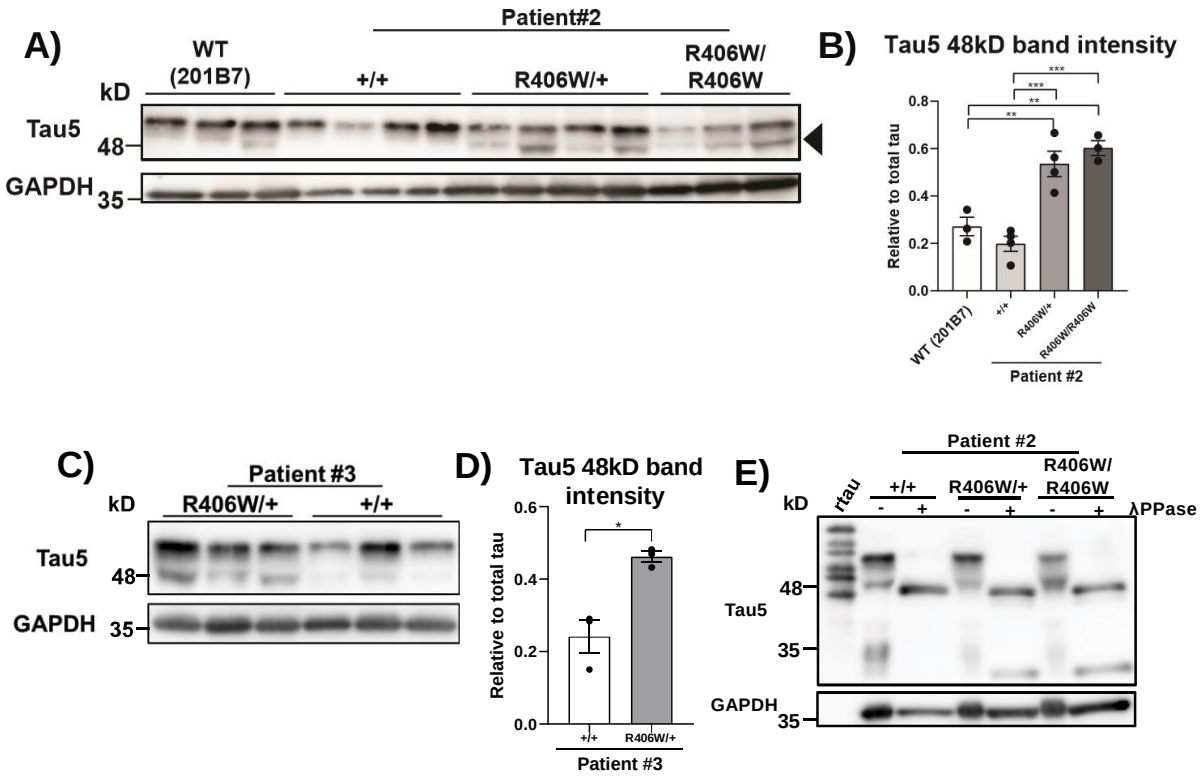

Figure 9. Mutant neurons exhibit increased amounts of hypophosphorylated tau.
Western blot with pan-tau antibody Tau5 revealed increased amounts of 48kD band in mutant neurons of both Patients #2 and #3 (A-D). Dephosphorylation of tau with λ-phosphatase (λPPase) confirmed that the lower 48kD band and upper 55kD band represent tau with different phosphorylation levels, with the 48kD band being the "hypophosphorylated" form of tau (E) (n=3; *p<0.05, **p<0.01, ***p<0.001).

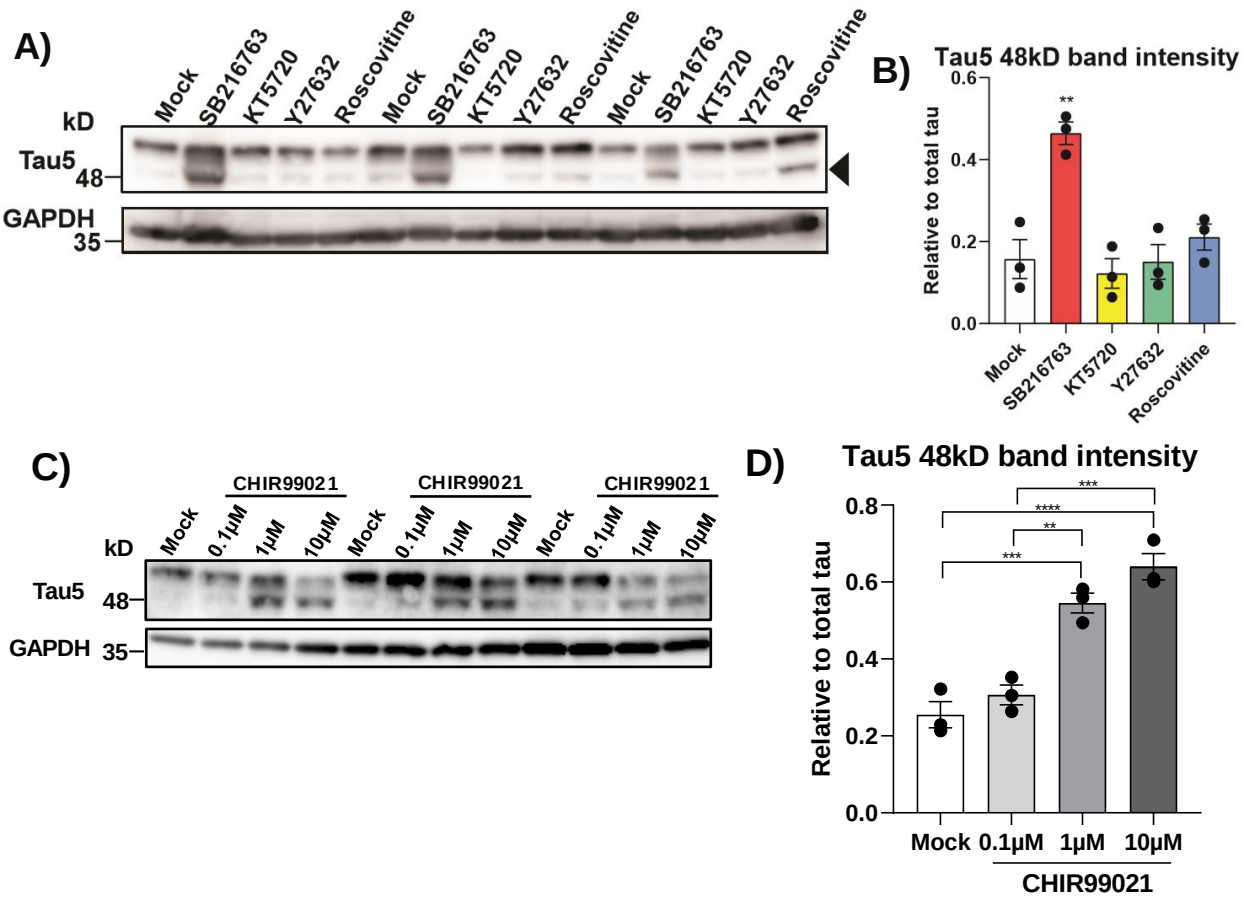

Figure 10. GSK3β is responsible for the reduced tau phosphorylation levels in the mutant neurons.

Western blot analysis investigating the effects of kinase inhibitors SB216763, KT5720, Y27632, and Roscovitine (inhibitors of GSK3β, PKA, RhoK, and CDK5, respectively) on the phosphorylation pattern of tau in WT (201B7) iPSC-derived neurons. The 48kD band intensity increased with SB216763 treatment only (A~B). Similar results were obtained with CHIR99021, another GSK3β inhibitor, with a dose-dependent increase of the 48kD band (C~D) (n=3; **p<0.01, ***p<0.001, ****p<0.0001).

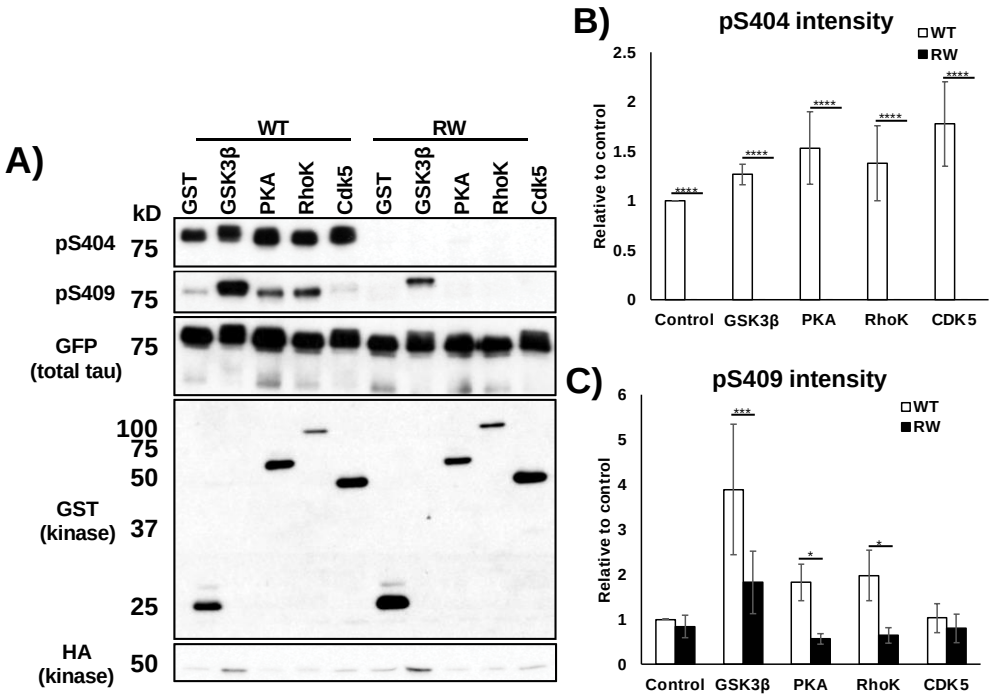

Figure 11. Phosphorylation of tau S404 and S409 epitopes by GSK3β is impaired with the R406W mutation

Western blot analysis of WT and R406W (RW) mutant tau conjugated with GFP and co-expressed with the respective kinases in COS-7 cells with tau antibodies detecting phosphorylation at S404 or S409. Both epitopes were phosphorylated by GSK3β in WT tau, but not as efficiently in RW tau (n=3; *p<0.05, ***p<0.001, ****p<0.0001).

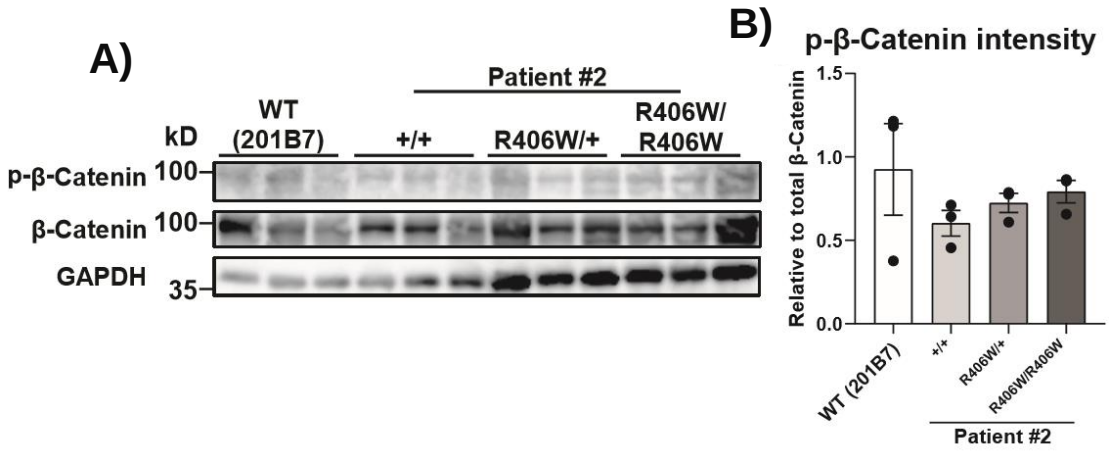

Figure 12. Phosphorylation of other GSK3β substrates besides tau remains unchanged. Western blot analysis of β-Catenin and p-β-Catenin (S33/S37/T41) levels in the iPSC-derived neurons. Levels of p-β-Catenin did not significantly differ among neuronal lines (n=3).

Increased fragmentation of R406W tau by calpain

Tau is reportedly cleaved by several proteases to produce tau fragments of different lengths[57]. Western blot analysis revealed an increase of tau fragments ranging from 35 kD to 45 kD in the R406W mutant samples across various epitopes (Figs. 13A~13F). This was especially evident when blotting with Tau12, which recognizes the N-terminus of tau, implying that the mutation particularly increases the generation of N-terminal tau fragments (Figs. 13A and 13B). Next, neurons were treated with inhibitors of the major proteases of tau—a pan-caspase inhibitor (Z-FAD-VMK) or a pan-calpain inhibitor (ALLN)—in order to identify which of these proteases was generating the fragments. Western blot analysis revealed a decrease of the 35kD fragment in samples treated with the calpain inhibitor, but not the caspase inhibitor Figs. 14A and 14B), indicating that calpain was generating the specific fragment. Interestingly, blotting with Tau5 revealed that the amount of hypophosphorylated tau (48kD) increased with calpain inhibition (Figs. 14C and 14D). These findings suggest that the 48kD hypophosphorylated tau was mainly fragmented by calpain and thus, the reduction of phosphorylation caused by the R406W mutation resulted in increased calpain cleavage of tau.

R406W mutation induces tau mislocalization and axonal dystrophy by MT destabilization

Dissociated neurons were further examined for phenotypes at the cellular level. Tau normally

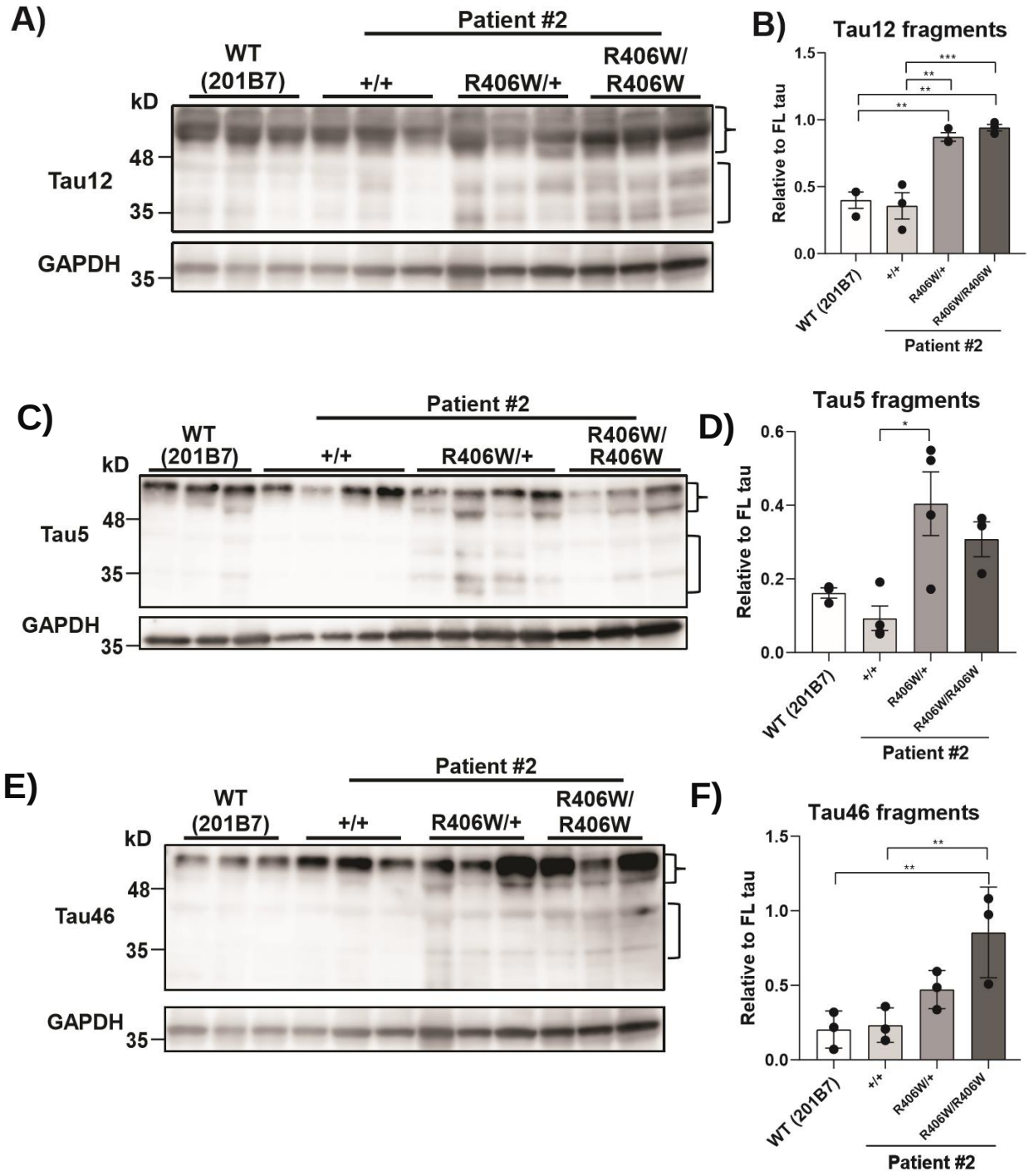

Figure 13. Increased tau fragments in R406W mutant neurons across various epitopes. Western blot analysis with pan-tau antibodies Tau12 (A~B), Tau5 (C~D), and Tau46 (E~F), which recognizes the N-terminus, mid-region, and C-terminus of tau, respectively, revealed that the *MAPT*$^{R406W/+}$ and *MAPT*$^{R406W/R406W}$ neurons have increased amounts of tau fragments ranging from 35kD to 45kD (n=3; *p<0.05, **p<0.01, ***p<0.001; brackets indicate tau fragments, braces indicate full-length (FL) tau).

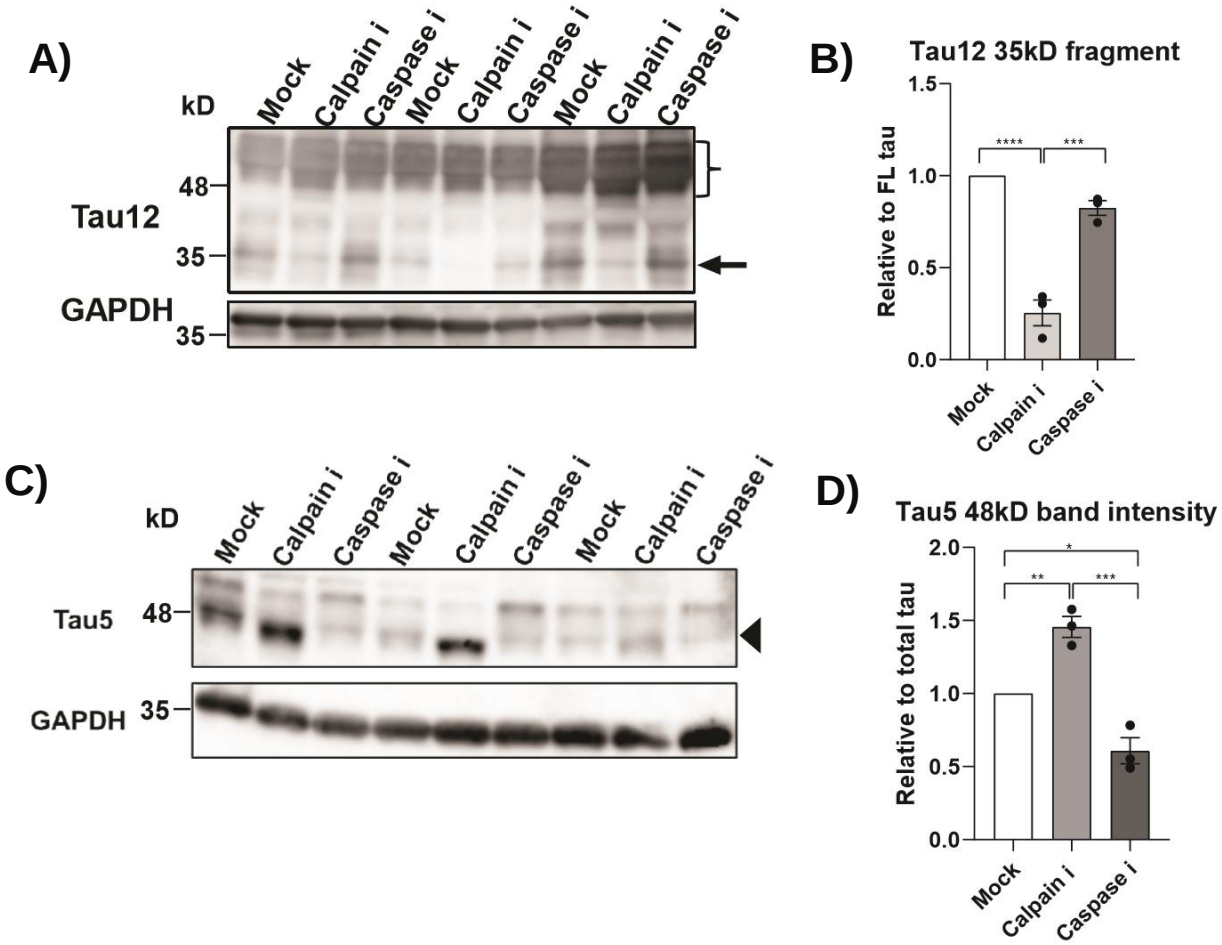

Figure 14. Increased fragmentation of R406W mutant tau by calpain is dependent on tau phosphorylation levels.

Calpain inhibition, but not caspase inhibition, decreased the amount of 35kD N-terminal tau fragments generated in the *MAPT*$^{R406W/R406W}$ neurons (A~B), while increasing the amount of the 48kD lower band, which represents hypophosphorylated tau (C~D) (n=3; *p<0.05, **p<0.01, ***p<0.001, ****p<0.0001).

localizes to the axons of neurons[20], but under pathological conditions, NFTs as well as abnormally phosphorylated tau were reported to accumulate in the somatodendritic compartments of neurons[34,58]. Furthermore, overexpression of mutant tau, but not WT tau, in rat primary neuronal culture resulted in the mislocalization of tau to the dendritic spines[59]. Thus, the localization of tau was investigated in the iPSC-derived neurons. Immunofluorescence of the neurons with tau and MAP2, a neuronal marker that specifically stains dendrites and cell bodies, revealed an increased colocalization of the two markers in the mutant neurons (Fig. 15A). Quantitative analysis confirmed that the mutant neurons had a small, but significant increase of tau on MAP2-positive dendrites at 30 days after dissociation (Fig. 15B). These results suggest that the R406W mutant tau is more likely to mislocalize from the axons to the dendrites of the neurons.

The morphology of the neurons was also investigated with immunofluorescence. Immunostaining with βIII-tubulin revealed a considerable number of dystrophic neurites in the mutant neurons (Fig. 16A). Such staining pattern was not observed with MAP2, indicating that the axons, but not the dendrites, were undergoing degeneration. At 30 days post dissociation, the axons of the mutant neurons consisted of a significantly greater number of small puncta (Figs. 16B and 16C). Interestingly, there were fewer axonal puncta when the mutant neurons were treated with Epothilone D (EpoD), a microtubule (MT) stabilizer (Figs. 16B and 16C). All together, these results implicate that the R406W mutant tau may cause axonal degeneration

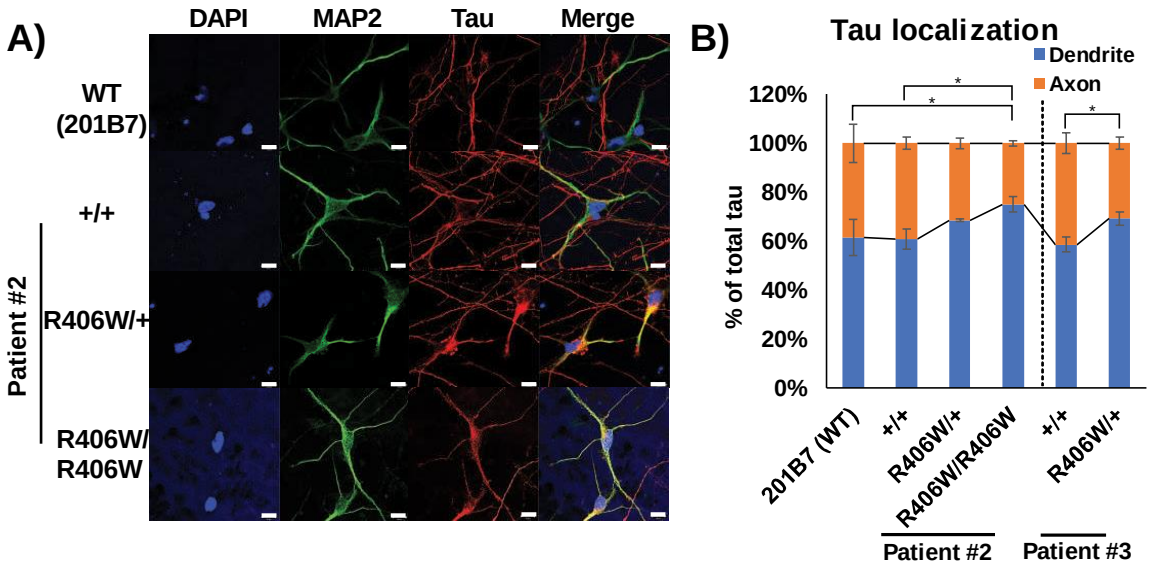

Figure 15. Mislocalization of tau in the R406W mutant neurons.

Co-localization of MAP2 and tau were more frequent in the *MAPT*$^{R406W/+}$ and *MAPT*$^{R406W/R406W}$ neurons (A) (Scale bar=10μm). In support of this, an increased percentage of tau was localized in the dendrites in the mutant neurons (B) (n=3; *p<0.05).

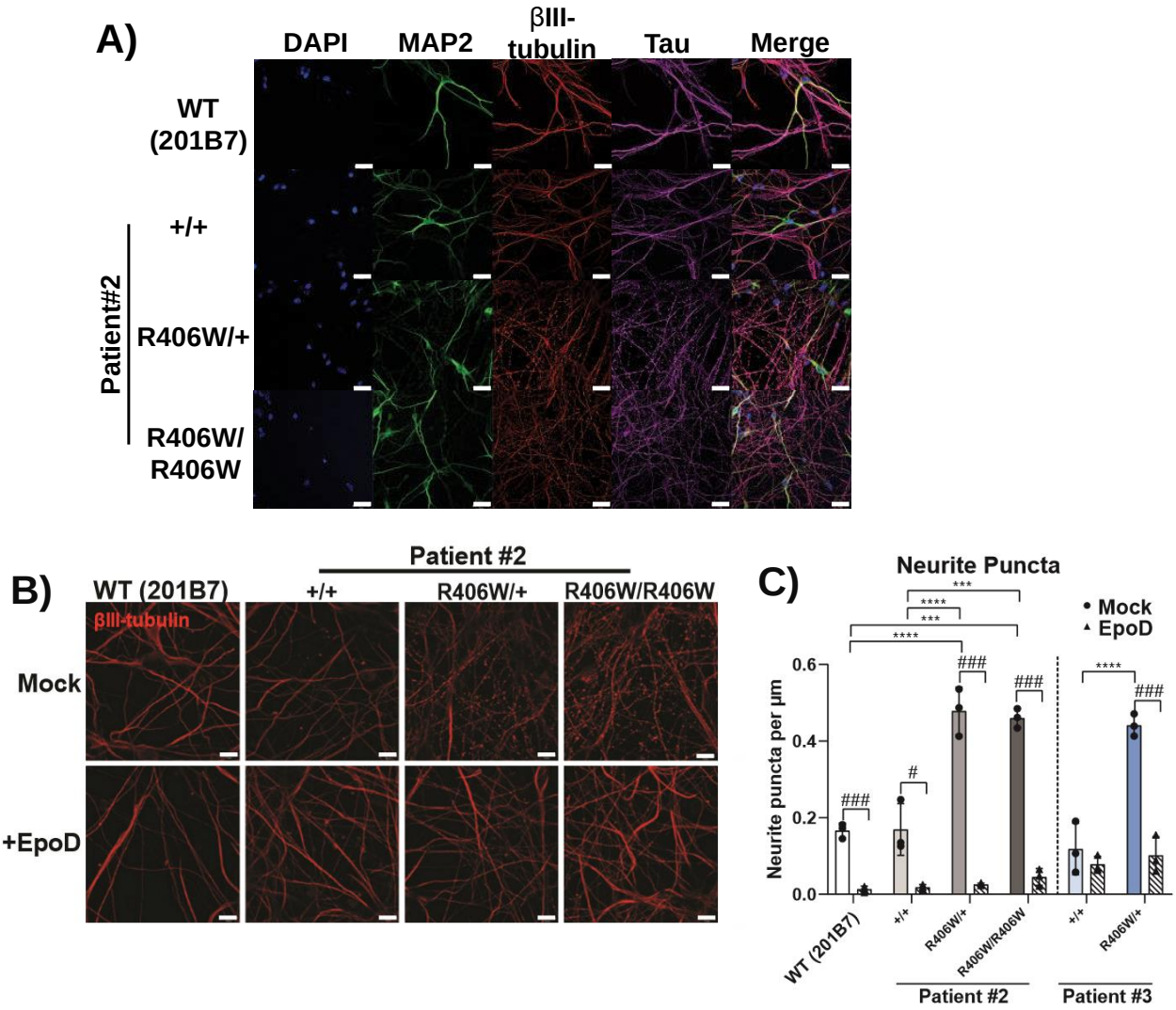

Figure 16. R406W mutant neurons exhibit dystrophic axons that can be rescued with microtubule stabilization.

MAP2(-)βIII-tubulin(+) axons of the *MAPT*$^{R406W/+}$ and *MAPT*$^{R406W/R406W}$ neurons were more dystrophic (A) (Scale bar=20µm). There were increased numbers of neurite puncta in these neurons, which was rescued with Epothilone D (EpoD) treatment (B~C) (n=3; ***p<0.001, ****p<0.0001 when comparing control vs R406W mutants; #p<0.05, ###p<0.001 when comparing mock vs EpoD).

by altering MT dynamics and/or stability.

MT destabilization disrupts mitochondrial transport in the mutant neurons

With axonal degeneration occurring in the mutant neurons, it was possible that the functional activity of the axons in these neurons were disrupted as well. Axonal transport is one such process responsible for carrying organelles and proteins within the neurons. Transport of mitochondria is particularly important, because neurons have high energy demands and require a large supply of ATP to maintain their function and survival[60]. As such, mitochondrial dysfunction has been implicated during the early stages of multiple neurodegenerative diseases[61]. Thus, mitochondrial transport function was analyzed in the iPSC-derived neurons. Neurons were transfected with Mito-eYFP and tdTomato for live imaging analysis of the mitochondria in intact axons. Here, mitochondria in the mutant neurons were found to be less stationary and moving more in the retrograde direction (Fig. 17A). In support of this data, fewer mitochondria were in the axons of the mutant neurons compared to those in the WT neurons, which again, was rescued with EpoD treatment (Figs. 17B and 17C). Overall, these results suggest that the R406W tau-induced MT destabilization caused an impairment in the axonal transport machinery.

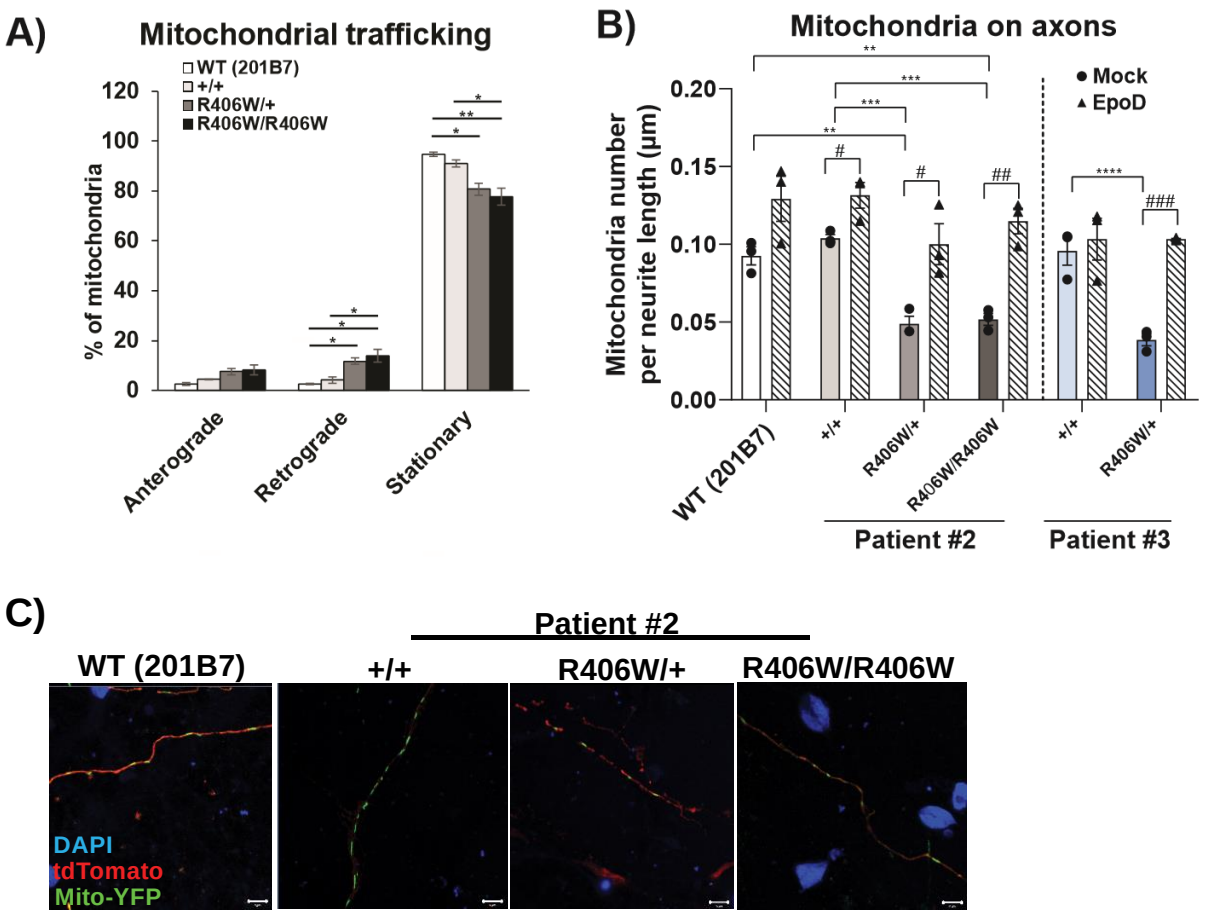

Figure 17. Microtubule destabilization causes mitochondrial transport defects in the R406W mutant neurons.

Mitochondrial trafficking analysis with live imaging revealed increased percentages of mitochondria moving in the retrograde direction in the R406W mutant neurons (A). Consistent with this data, there were fewer mitochondria in the axons of the mutant neurons, but the number recovered to the control level with EpoD treatment (B~C) (n=3; **<p.001, ***p<0.001, ****p<0.0001 when comparing control vs R406W mutants; #p<0.05, ##p<0.01, ###p<0.001 when comparing mock vs EpoD)

Temporal progression of phenotypes in the iPSC-derived neurons

Finally, in order to investigate the temporal progression of the phenotypes identified in the iPSC-derived neurons, the phenotypes described above were assessed at an earlier timepoint of 10 days post dissociation. Although tau phosphorylation levels were already reduced in the R406W mutant neurons (Fig. 18), tau mislocalization and axonal dystrophy were not observed at this timepoint (Fig. 19). Therefore, the abnormal reduction of tau phosphorylation precedes the cellular phenotypes in the iPSC-derived mutant neurons.

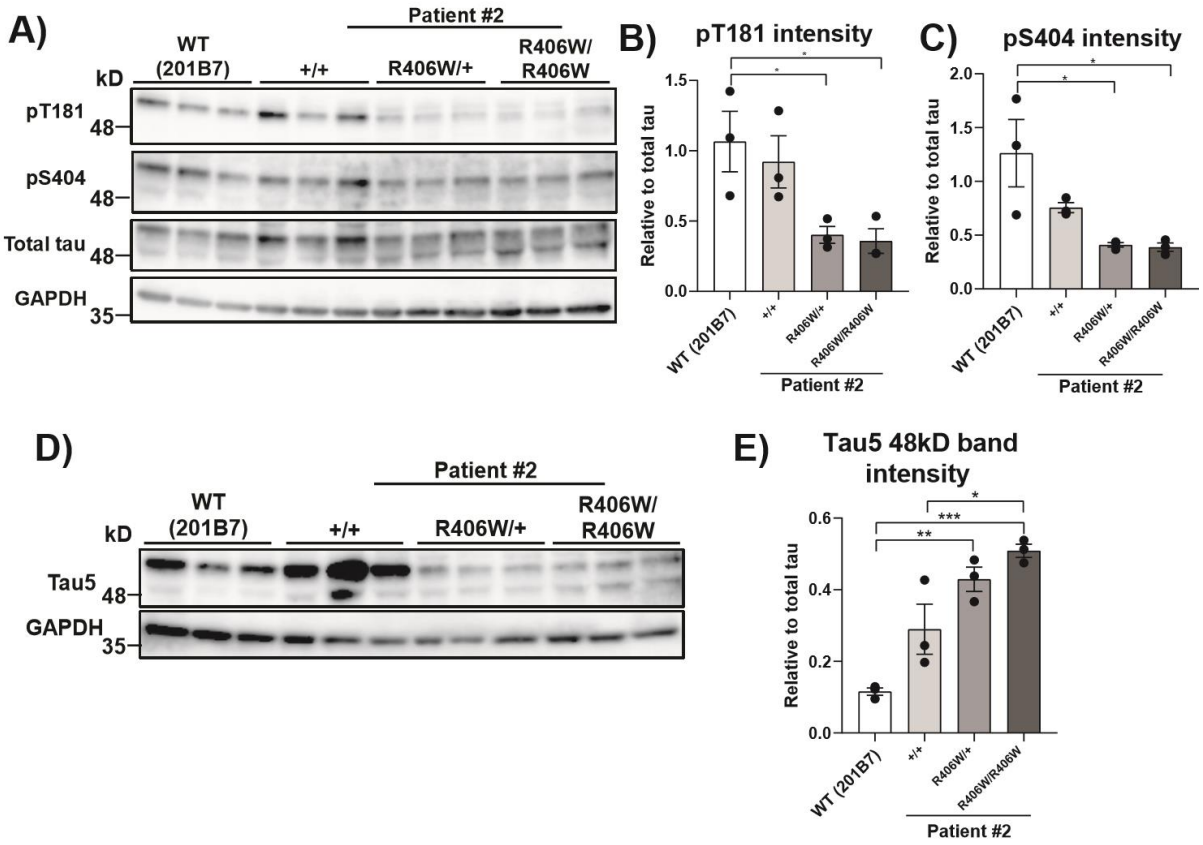

Figure 18. Tau phosphorylation is already reduced in R406W mutant neurons at an early timepoint.

At 10 days post dissociation, the tau phosphorylation levels at T181 and S404 were reduced (A~C) and there were increased amounts of 48kD hypophosphorylated tau (D~E) in the *MAPT*$^{R406W/+}$ and *MAPT*$^{R406W/R406W}$ neurons (n=3; *p<0.05, **p<0.01, ***p<0.001).

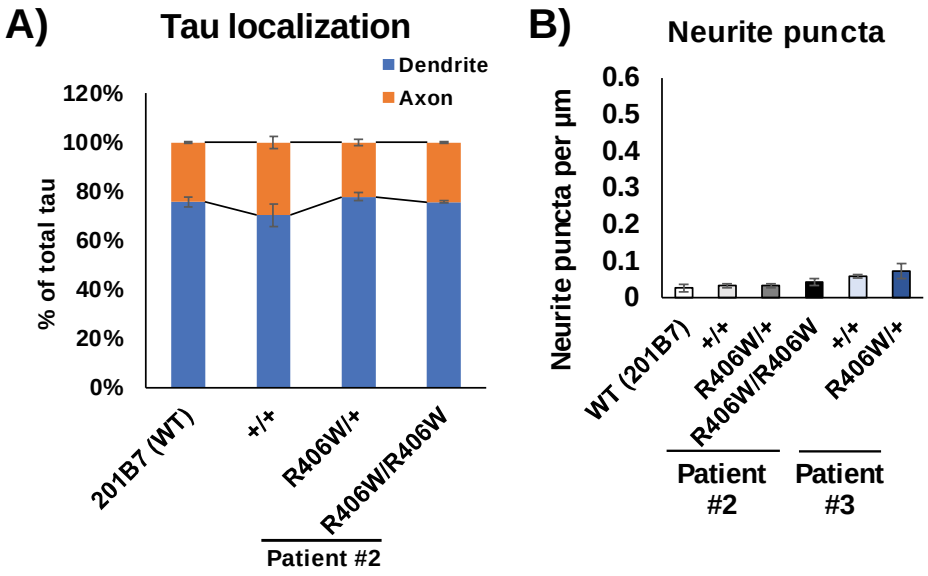

Figure 19. Cellular phenotypes are not observed in R406W mutant neurons at earlier timepoints.

At 10 days post dissociation, tau mislocalization to the dendrites (A) or increase in neurite puncta (B) were not observed in the R406W mutant neurons.

Discussion

The role of tau in neurodegeneration has been extensively studied using various models. Development of tau transgenic animal models and cell line models has provided fundamental insight of tau under both physiological and pathological conditions[34~36,62,63]. In the case of R406W mutant tau, hyperphosphorylation and aggregation of tau into filament-like structures[64,65], as well as retardation of axonal transport[66] has been reported in R406W tau transgenic mice. In cell line models, soluble R406W tau was less phosphorylated and its binding to microtubules was reduced[67-71]. However, despite intensive studies, these findings have not translated well into the clinics, as proven by the repeated failures of promising therapeutics in recent years. It is necessary to further elucidate the pathological mechanism of the disease using an improved model that better recapitulates the pathology of the patients. So far, the number of studies using a human-based model to investigate the *MAPT* R406W mutation has been limited[52,72]. Therefore, in this study, a patient-derived neuronal model was developed using the iPSC technology to recapture the disease pathology induced by the *MAPT* R406W mutation.

Taking advantage of the CRISPR/Cas9 gene-editing technology and PiggyBac transposase system[46,53], footprint-free isogenic WT ($MAPT^{+/+}$) or homozygous ($MAPT^{R406W/R406W}$) iPSC lines were established from the original heterozygous R406W ($MAPT^{R406W/+}$) patient-derived iPSC lines. These lines have a genetically identical background, making them important tools for assessing the genotype-phenotype relationship.

Using previously reported protocols, the iPSC lines were induced into cerebral organoids[47,48]. Building upon this approach, a novel method was devised for isolating a homogenous population of cortical neurons from the organoids. With this protocol, a high percentage of cells expressing pan-neuronal markers (>85~90%) and forebrain markers (~80%) was obtained without the use of transgenes, which enable rapid, robust induction of neuronal cells, but of unknown identity, as opposed to neurons of this study[73]. There were also high expression levels of NeuN, indicating the presence of mature neurons. Furthermore, a great number of neurons could be obtained by dissociating a bulk of organoids and it is possible to regulate this number by manipulating the number of organoids to be dissociated, making this method feasible for various types of analyses. This is the first time that dissociated organoids were used for disease modeling, and the results from this study clearly showed that the dissociated culture is suitable for both biochemical and immunochemical analyses. Hence, the utility of organoids for application besides 3D modeling was demonstrated.

Using the neuronal culture described above, the phosphorylation state of the mutant tau was first examined. Abnormal phosphorylation of tau is a pathological hallmark of AD and other tauopathies, which is known to further trigger tau pathology by reducing its affinity to microtubules, enhancing aggregation, altering its interactions with other proteins, and missorting it from axons to the somatodendritic compartments in neurons[74]. There have been several findings reporting the aberrant phosphorylation status of R406W mutant tau, but results

have been controversial. Results from *in vitro* experiments and non-neuronal cell lines indicated R406W mutant tau to be less phosphorylated than wild-type tau[56,64,68-70], while studies using murine models or post-mortem R406W patient brains claimed that they were hyperphosphorylated[65,67,71,75]. These controversies may have arisen because of the differences in tau solubility and the disease stages reflected in each model. In the human iPSC-derived neuronal model of this study, R406W mutant tau was found to be less phosphorylated at specific epitopes. In addition to demonstrating reduced phosphorylation at T181 and S404, S409 was newly identified to be less phosphorylated in the mutant tau using western blot analyses. Using *in vitro* experiments, it was further revealed that the mutation impaired phosphorylation by PKA, RhoK, and GSK3β at these epitopes. In particular, GSK3β accounted for the overall reduction of phosphorylation, which is supported by the fact that T181, S404, and S409 are all potential phosphorylation sites by this kinase[76]. However, it should be noted that the reduction of phosphorylation at S404 is debatable, when taking into consideration a change in immunogenicity due to the mutation. Nevertheless, based on these findings and those from previous reports, it is highly plausible that the arginine-to-tryptophan substitution makes tau less prone to phosphorylation by specific kinases, possibly due to some conformational change of the mutant tau. However, as the disease progresses, the mutant tau may become hyperphosphorylated, due to an unknown mechanism not identified yet, as seen in the murine models and patient brains[65,67,71,75].

In this current study, tau phosphorylation was mainly examined by western blotting. Interestingly, during the course of analyses, *MAPT* $^{R406W/+}$ and *MAPT* $^{R406W/R406W}$ lines of Patient #2 were revealed to have increased GAPDH levels (Figs. 7A, 7G, 9A, 12A, 13A, 13C, 13E). This did not appear to be a genotype-dependent phenomenon, as it was not observed with cell lines from Patient #3 (Figs. 7E, 9C). A similar increase of expression was found in the mutants of Patient #2 for other housekeeping genes, including β-actin and α-tubulin (data not shown). One possible explanation for this is different levels of cell confluence among the neuronal lines. Greer et al. demonstrated that cell density can affect the expression of housekeeping genes, including GAPDH[77]. In this study, when plating the same number of cells after dissociating the organoids derived from Patient #2, the mutants tended to have a higher cell density than the controls. Thus, it may be possible that the elevated GAPDH level in the mutants of Patient #2 is simply a reflection of high cell density.

Results regarding the efficiency of R406W mutant tau to bind and/or assemble microtubules compared to WT tau has also been controversial[69-71,78-80]. Here, the mutant tau was found to induce cellular phenotypes through the destabilization of microtubules. These phenotypes were rescued with the treatment of microtubule stabilizer Epothilone D (EpoD), suggesting that the R406W mutation exerts negative effects on the physiological interaction of tau with microtubules.

Investigation at the cellular level revealed the mislocalization of tau to the dendrites

and more punctuate axons in the mutant neurons, both of which have been observed in AD brains[58]. Furthermore, there was a decrease in the number of mitochondria on the axons of the mutant neurons. Impairment of mitochondrial distribution has also been reported in the rTg4510 mouse model, which overexpresses the P301L mutant tau protein, and in AD patient brains[810], as well as in a P301L tau knock-in mouse model, which has also interestingly found elevated amounts of hypophosphorylated tau[82]. In addition, live imaging analysis showed that mitochondria in the mutant neurons were less stationary, and an increased percentage moved more in the retrograde direction away from the axons, which is consistent with the reduction of its number in the axons. This is in contrast to a previous study also using FTDP-17 patient-derived iPSC-neurons, reporting that mitochondria in the mutant neurons were less mobile[83]. This discrepancy may be due to the differences in the mutations analyzed (R406W in this study versus P301L, N279K in Ref. 83). A previous report has demonstrated that microtubule-bound tau inhibits the motility of motor proteins kinesin and dynein, and that the microtubule binding domain (MTBD) of tau is sufficient for this inhibition[84]. Thus, the impaired association of R406W tau with MTs may have promoted dynein to become overly motile, resulting in the increase of retrograde movement of mitochondria. In support of this, the axonal mitochondrial number in the mutant neurons was rescued with EpoD treatment, confirming that MT destabilization induced by the mutant tau caused the transport defect.

Despite the numerous reports on tau pathology, the pathological cascade leading to

neurodegeneration is still unknown. For example, the specific role of aberrant tau phosphorylation during pathological progression remains widely unexplored. Results from this study implicated that reduced tau phosphorylation makes tau more susceptible to calpain cleavage to generate 35kD N-terminal fragments. The calpain cleavage site of tau has been reported to be near or inside the MTBD[85,86]. Therefore, the resultant tau fragment either may have lost its ability to stabilize microtubules or have gained a toxic function to destabilize them, ultimately triggering the axonal phenotypes. Furthermore, although the cellular phenotypes could be observed in the mutant neurons at 30 days after dissociation, they could not be detected at an earlier timepoint. However, tau hypophosphorylation already occurred at 10 days post dissociation. Thus, abnormal tau phosphorylation seen in this study could be an early hallmark of the disease that triggers fragmentation of tau by calpain, which further induces MT destabilization, leading to axonal dystrophy and axonal transport defects.

This study describes a previously unidentified molecular mechanism of tau pathology specifically induced by the R406W mutation. The use of patient-matched neurons not only provided new discoveries into tau pathology, but also novel interpretations regarding previous controversial results. In summary, understanding the cascade of pathological events leading to neurodegeneration using iPSC-derived models will help in defining targets for therapeutic development for a wide variety of tauopathies and other neurodegenerative diseases

Conclusion

In this present study, isogenic panels of iPSC lines were established from FTDP-17 patients carrying the *MAPT* R406W mutation. These iPSC lines were induced into a homogenous population of cortical neurons by dissociating cerebral organoids. In this neuronal culture, R406W mutant tau was found to exhibit decreased phosphorylation levels, which likely causes increased fragmentation of tau by calpain. In addition, examination at the cellular level revealed an increased amount of tau in the dendrites of the patient neurons as well as axonal degeneration and mitochondrial transport defects induced by the mutant tau through the destabilization of microtubules. These features could represent some of the early pathological hallmarks of FTDP-17 with the *MAPT* R406W mutation. As such, clarifying the pathological molecular mechanism of neurodegeneration using iPSC-derived patient neuronal models could facilitate our understanding of disease onset and progression, and ultimately contribute to novel therapeutic development for dementia and other neurodegenerative diseases.

Acknowledgments

Firstly, I am grateful for Dr. Hideyuki Okano of Keio University for accepting me into his laboratory to work on this project and for giving me many valuable advices and support. I would also like to thank my adviser Dr. Seiji Shiozawa of Keio University for providing tremendous assistance and dedicated involvement in every step during the project, as well as all of the other members of the Okano laboratory for their critical advices and support.

I must also thank Dr. Takeshi Ikeuchi of Niigata University for providing me the blood samples from FTDP-17 patients carrying the *MAPT* R406W mutation, Dr. Celeste M. Karch of Washington University in St. Louis for providing additional isogenic *MAPT* R406W iPSC lines, and Dr. Shinya Yamanaka of Kyoto University for providing the 201B7 iPSC line. This research could not have been done without their contributions.

In addition, I would like to show gratitude to Drs. Kozo Kaibuchi, Daisuke Tsuboi, and Mutsuki Amano of Nagoya University for providing data regarding tau phosphorylation and *in vitro* kinase assays, and also to Drs. Shin-ichi Hisanaga and Taeko Kimura of Tokyo Metropolitan University for their support in analyzing tau phosphorylation. I would also like to thank Dr. Naruhiko Sahara for taking time to teach me western blotting of tau at the National Institute of Radiological Sciences, and for providing tau antibodies. I would also like to express gratitude towards Dr. Tomohiro Miyasaka of Doshisha Univeristy for providing tau antibodies and for his support in analyzing tau localization, and Dr. Akihiko Takashima of Gakushuuin

University for giving me advice on analytical methods. I am also grateful to Drs. Takami Tomiyama and Tomohiro Umeda for providing the pcDNA3 Mito-eYFP construct.

Lastly, I would like to thank Dr. Youichi Watanabe of the Department of Biomedical Chemistry for being my research supervisor and his wonderful assistance and understanding in conducting the research, as well as all of the other members of the lab for their critical advices and comments.

This study was supported by the Acceleration Program for Intractable Disease Research Utilizing Disease-specific iPS Cells from the Japan Agency for Medical Research and Development (Grant No. 19bm0804003h0003) and by the Scientific Research in Innovative Areas “Brain Protein Aging and Dementia Control” from the MEXT. The generation of the iPSC lines (Patient #3) was supported by grants from the National Institutes of Health (K01 AG046374 and P50 AG005681).

References

1. Plassman, B. L., Langa, K. M., Fisher, G. G., Heeringa, S. G., Weir, D. R., Ofstedal, M. B., Burke, J. R., Hurd, M. D., Potter, G. G., Rodgers, W. L., Steffens, D. C, Willis, R. J., and Wallace, R. B. Prevalence of dementia in the United States: the aging, demographics, and memory study. *Neuroepidemiology*, *29*(1-2), 125-132 (2007).
2. Hebert, L. E., Weuve, J., Scherr, P. A., and Evans, D. A. Alzheimer disease in the United States (2010–2050) estimated using the 2010 census. *Neurology*, *80*(19), 1778-1783 (2013).
3. Gaugler, J., James, B., Johnson, T., Marin, A., and Weuve, J. 2019 Alzheimer's disease facts and figures. *Alzheimers & Dementia*, *15*(3), 321-387 (2019).
4. Prince, M. J. World Alzheimer Report 2015: the global impact of dementia: an analysis of prevalence, incidence, cost and trends. Alzheimer's Disease International (2015).
5. Alzheimer, A. Uber einen eigenartigen schweren Er Krankungsprozeb der Hirnrinde. *Neurologisches Centralblatt*, *23*, 1129-1136 (1906).
6. Glenner, G. G., and Wong, C. W. Alzheimer's disease: initial report of the purification and characterization of a novel cerebrovascular amyloid protein. *Biochemical and Biophysical Research Communications*, *120*(3), 885-890 (1984).
7. Nukina, N., and Ihara, Y. One of the antigenic determinants of paired helical filaments is related to tau protein. *The Journal of Biochemistry*, *99*(5), 1541-1544 (1986).

8. Grundke-Iqbal, I., Iqbal, K., Quinlan, M., Tung, Y. C., Zaidi, M. S., and Wisniewski, H. M. Microtubule-associated protein tau. A component of Alzheimer paired helical filaments. *Journal of Biological Chemistry*, *261*(13), 6084-6089 (1986).
9. Grundke-Iqbal, I., Iqbal, K., Tung, Y. C., Quinlan, M., Wisniewski, H. M., and Binder, L. I. Abnormal phosphorylation of the microtubule-associated protein tau (tau) in Alzheimer cytoskeletal pathology. *Proceedings of the National Academy of Sciences*, *83*(13), 4913-4917 (1986).
10. Jack Jr, C. R., Knopman, D. S., Jagust, W. J., Shaw, L. M., Aisen, P. S., Weiner, M. W., Peterson, R. C., and Trojanowski, J. Q. Hypothetical model of dynamic biomarkers of the Alzheimer's pathological cascade. *The Lancet Neurology*, *9*(1), 119-128 (2010).
11. Goate, A., Chartier-Harlin, M. C., Mullan, M., Brown, J., Crawford, F., Fidani, L., Giuffra, L., Haynes, A., Irving, N., James, L., Mant, R., Newton, P., Rooke, K., Roques, P., Talbot, C., Pericak-Vance, M., Roses, A., Williamson, R., Rossor, M., Owen, M., and Hardy, J. Segregation of a missense mutation in the amyloid precursor protein gene with familial Alzheimer's disease. *Nature*, *349*(6311), 704 (1991).
12. Sherrington, R., Rogaev, E. I., Liang, Y., Rogaeva, E. A., Levesque, G., Ikeda, M., Chi, H., Lin, C., Li, G., Holman, K., Tsuda, T., Mar, L., Foncin, J.-F., Bruni, A. C., Montesi, M. P., Sorbi, S., Rainero, I., Pinessi, L., Nee, L., Chumakov, I., Pollen, D., Brookes, A., Sanseau, P., Polinsky, R. J., Wasco, W., Da Silva, H. A. R., Haines, J. L., Pericak-Vance,

M. A., Tanzi, R. E., Roses, A. D., Fraser, P. E., Rommens, J. M., and St. George-Hyslop, P. H.. Cloning of a gene bearing missense mutations in early-onset familial Alzheimer's disease. *Nature*, *375*(6534), 754 (1995).

13. Levy-Lahad, E., Wijsman, E. M., Nemens, E., Anderson, L., Goddard, K. A., Weber, J. L., Bird, T. D., and Schellenberg, G. D. A familial Alzheimer's disease locus on chromosome 1. *Science*, *269*(5226), 970-973 (1995).
14. Hardy, J. A., and Higgins, G. A. Alzheimer's disease: the amyloid cascade hypothesis. *Science*, *256*(5054), 184-186 (1992).
15. Giacobini, E., and Gold, G. Alzheimer disease therapy—moving from amyloid-β to tau. *Nature Reviews Neurology*, *9*(12), 677 (2013).
16. Mullane, K., and Williams, M. Alzheimer's therapeutics: continued clinical failures question the validity of the amyloid hypothesis—but what lies beyond?. *Biochemical Pharmacology*, *85*(3), 289-305 (2013).
17. Arriagada, P. V., Growdon, J. H., Hedley-Whyte, E. T., and Hyman, B. T. Neurofibrillary tangles but not senile plaques parallel duration and severity of Alzheimer's disease. *Neurology*, *42*(3), 631-631 (1992).
18. Giannakopoulos, P., Herrmann, F. R., Bussière, T., Bouras, C., Kövari, E., Perl, D. P., Morrison, J. H., Gold, G., and Hof, P. R. Tangle and neuron numbers, but not amyloid load, predict cognitive status in Alzheimer’s disease. *Neurology*, *60*(9), 1495-1500 (2003).

19. Weingarten, M. D., Lockwood, A. H., Hwo, S. Y., and Kirschner, M. W. A protein factor essential for microtubule assembly. *Proceedings of the National Academy of Sciences*, *72*(5), 1858-1862 (1975).

20. Binder, L. I., Frankfurter, A., and Rebhun, L. I. The distribution of tau in the mammalian central nervous system. *The Journal of Cell Biology*, *101*(4), 1371-1378 (1985).

21. Lee, V. M., Goedert, M., and Trojanowski, J. Q. Neurodegenerative tauopathies. *Annual Review of Neuroscience*, *24*(1), 1121-1159 (2001).

22. De Calignon, A., Polydoro, M., Suárez-Calvet, M., William, C., Adamowicz, D. H., Kopeikina, K. J., Pitstick, R., Sahara, N., Ashe, K. H., Carlson, G. A., Spires-Jones, T. L., and Hyman, B. T. Propagation of tau pathology in a model of early Alzheimer's disease. *Neuron*, *73*(4), 685-697 (2012).

23. Poorkaj, P., Bird, T. D., Wijsman, E., Nemens, E., Garruto, R. M., Anderson, L., and Schellenberg, G. D. Tau is a candidate gene for chromosome 17 frontotemporal dementia. *Annals of Neurology*, *43*(6), 815-825 (1998).

24. Hutton, M., Lendon, C. L., Rizzu, P., Baker, M., Froelich, S., Houlden, H., and Hackett, J. Association of missense and 5′-splice-site mutations in tau with the inherited dementia FTDP-17. *Nature*, *393*(6686), 702-705 (1998).

25. Spillantini, M. G., Murrell, J. R., Goedert, M., Farlow, M. R., Klug, A., and Ghetti, B. Mutation in the tau gene in familial multiple system tauopathy with presenile dementia.

Proceedings of the National Academy of Sciences, *95*(13), 7737-7741 (1998).

26. Ghetti, B., Oblak, A. L., Boeve, B. F., Johnson, K. A., Dickerson, B. C., and Goedert, M. Invited review: Frontotemporal dementia caused by microtubule-associated protein tau gene (MAPT) mutations: a chameleon for neuropathology and neuroimaging. *Neuropathology and Applied Neurobiology*, *41*(1), 24-46 (2015).
27. Ghetti, B., Wszolek, Z. K., and Boeve, B. F. *Neurodegeneration: The Molecular Pathology of Dementia and Movement Disorders*. 2nd ed. 14 Frontotemporal Dementia and Parkinsonism Linked to Chromosome 17. Dickson, Dennis, and Roy O. Weller, eds. United Kingdom: Wiley-Blackwell (an imprint of John Wiley & Sons Ltd) (2011). Print.
28. Rizzu, P., Van Swieten, J. C., Joosse, M., Hasegawa, M., Stevens, M., Tibben, A. and Goedert, M. High prevalence of mutations in the microtubule-associated protein tau in a population study of frontotemporal dementia in the Netherlands. *The American Journal of Human Genetics*, *64*(2), 414-421 (1999).
29. Van Swieten, J. C., Stevens, M., Rosso, S. M., Rizzu, P., Joosse, M., De Koning, I. and Heutink, P. Phenotypic variation in hereditary frontotemporal dementia with tau mutations. *Annals of Neurology*, *46*(4), 617-626 (1999).
30. Reed, L. A., Schelper, R. L., Solodkin, A., Van Hoesen, G. W., Morris, J. C., Trojanowski, J. Q., and Wragg, M. A. Autosomal dominant dementia with widespread neurofibrillary tangles. *Annals of Neurology*, *42*(4), 564-572 (1997).

31. Saito, Y., Geyer, A., Sasaki, R., Kuzuhara, S., Nanba, E., Miyasaka, T., and Murayama, S. Early-onset, rapidly progressive familial tauopathy with R406W mutation. *Neurology*, *58*(5), 811-813 (2002).

32. Foster, N. L., Wilhelmsen, K., Sima, A. A., Jones, M. Z., D'Amato, C. J., and Gilman, S. Frontotemporal dementia and parkinsonism linked to chromosome 17: a consensus conference. *Annals of Neurology*, *41*(6), 706-715 (1997).

33. Ikeuchi, T., Imamura, T., Kawase, Y., Kitade, Y., Tsuchiya, M., Tokutake, T. and Sugishita, M. Evidence for a common founder and clinical characteristics of Japanese families with the MAPT R406W mutation. *Dementia and Geriatric Cognitive Disorders Extra*, *1*(1), 267-275 (2011).

34. Götz, J., Probst, A., Spillantini, M. G., Schäfer, T., Jakes, R., Bürki, K., and Goedert, M. Somatodendritic localization and hyperphosphorylation of tau protein in transgenic mice expressing the longest human brain tau isoform. *The EMBO Journal*, *14*(7), 1304-1313 (1995).

35. Lewis, J., McGowan, E., Rockwood, J., Melrose, H., Nacharaju, P., Van Slegtenhorst, M., Gwinn-Hardy, K., Murphy, M. P., Baker, M., Yu, X., Duff, K., Hardy, J., Corral, A., Lin, W.-L., Yen, S.-H., Dickson, D. W., Davies, P., and Hutton, M. Neurofibrillary tangles, amyotrophy and progressive motor disturbance in mice expressing mutant (P301L) tau protein. *Nature Genetics*, *25*(4), 402 (2000).

36. Yoshiyama, Y., Higuchi, M., Zhang, B., Huang, S. M., Iwata, N., Saido, T. C., Maeda, J., Suhara, T., Trojanowski, J. Q., and Lee, V. M. Y. Synapse loss and microglial activation precede tangles in a P301S tauopathy mouse model. *Neuron*, *53*(3), 337-351 (2007).

37. Takahashi, K. and Yamanaka, S. Induction of pluripotent stem cells from mouse embryonic and adult fibroblast cultures by defined factors. *Cell*, *126*(4), 663-676 (2006).

38. Takahashi, K., Tanabe, K., Ohnuki, M., Narita, M., Ichisaka, T., Tomoda, K., and Yamanaka, S. Induction of pluripotent stem cells from adult human fibroblasts by defined factors. *Cell*, *131*(5), 861-872 (2007).

39. Evans, M. J., and Kaufman, M. H. Establishment in culture of pluripotential cells from mouse embryos. *Nature*, *292*(5819), 154 (1981).

40. Kriks, S., Shim, J. W., Piao, J., Ganat, Y. M., Wakeman, D. R., Xie, Z., Carrillo-Reid, L., Auyeung, G., Antonacci, C., Buch, A., Yang, L., Beal, M. F., Surmeier, D. J., Kordower, J. H., Tabar, V., and Studer, L. Dopamine neurons derived from human ES cells efficiently engraft in animal models of Parkinson's disease. *Nature*, *480*(7378), 547 (2011).

41. Hallett, P. J., Deleidi, M., Astradsson, A., Smith, G. A., Cooper, O., Osborn, T. M., Sundberg, M., Moore, M. A., Perez-Torres, E., Brownell, A.-L., Schumacher, J. M., Spealman, R. D., and Isacson, O. Successful function of autologous iPSC-derived dopamine neurons following transplantation in a non-human primate model of Parkinson's disease. *Cell Stem Cell*, *16*(3), 269-274 (2015).

42. Nori, S., Okada, Y., Yasuda, A., Tsuji, O., Takahashi, Y., Kobayashi, Y., Fujiyoshi, K., Koike, M., Uchiyama, Y., Ikeda, E., Toyama, Y., Yamanaka, S., Nakamura, M., and Okano, H. Grafted human-induced pluripotent stem-cell–derived neurospheres promote motor functional recovery after spinal cord injury in mice. *Proceedings of the National Academy of Sciences*, *108*(40), 16825-16830 (2011).

43. Mandai, M., Watanabe, A., Kurimoto, Y., Hirami, Y., Morinaga, C., Daimon, T., Fujihara, M., Akimaru, H., Sakai, N., Shibata, Y., Terada, M., Nomiya, Y., Tanishima, S., Nakamura, M., Kamao, H., Sugita, S., Onishi, A., Ito, T., Fujita, K., Kawamata, S., Go, M. J., Shinohara, C., Hata, K., Sawada, M., Yamamoto, M., Ohta, S., Ohara, Y., Yoshida, K., Kuwahara, J., Kitano, Y., Amano, N., Umekage, M., Kitakoka, F., Tanaka, A., Okada, C., Takasu, N., Ogawa, S., Yamanaka, S., and Takahashi, M. Autologous induced stem-cell–derived retinal cells for macular degeneration. *New England Journal of Medicine*, *376*(11), 1038-1046 (2017).

44. Okita, K., Yamakawa, T., Matsumura, Y., Sato, Y., Amano, N., Watanabe, A., and Yamanaka, S. An efficient nonviral method to generate integration-free human-induced pluripotent stem cells from cord blood and peripheral blood cells. *Stem Cells*, *31*(3), 458-466 (2013).

45. Ichiyanagi, N., Fujimori, K., Yano, M., Ishihara-Fujisaki, C., Sone, T., Akiyama, T., Okada, Y., Akamatsu, W., Matsumoto, T., Ishikawa, M., Nishimoto, Y., Ishihara, Y., Sakuma, T., Yamamoto, T., Tsuiji, H., Suzuki, N., Warita, H., Aoki, M., and Okano, H. Establishment of

in vitro FUS-associated familial amyotrophic lateral sclerosis model using human induced pluripotent stem cells. *Stem Cell Reports*, *6*(4), 496-510 (2016).

46. Nakamoto, F. K., Okamoto, S., Mitsui, J., Sone, T., Ishikawa, M., Yamamoto, Y., Kanegae, Y., Nakatake, Y., Imaizumi, K., Ishiura, H., Tsuji, S., and Okano, H. The pathogenesis linked to coenzyme Q10 insufficiency in iPSC-derived neurons from patients with multiple-system atrophy. *Scientific Reports*, *8*(1), 14215 (2018).

47. Lancaster, M. A., Renner, M., Martin, C. A., Wenzel, D., Bicknell, L. S., Hurles, M. E., and Knoblich, J. A. Cerebral organoids model human brain development and microcephaly. *Nature*, *501*(7467), 373-379 (2013).

48. Kadoshima, T., Sakaguchi, H., Nakano, T., Soen, M., Ando, S., Eiraku, M., and Sasai, Y. Self-organization of axial polarity, inside-out layer pattern, and species-specific progenitor dynamics in human ES cell–derived neocortex. *Proceedings of the National Academy of Sciences*, *110*(50), 20284-20289 (2013).

49. Watanabe, K., Ueno, M., Kamiya, D., Nishiyama, A., Matsumura, M., Wataya, T., and Sasai, Y. A ROCK inhibitor permits survival of dissociated human embryonic stem cells. *Nature Biotechnology*, *25*(6), 681-686 (2007).

50. Amano, M., Kaneko, T., Maeda, A., Nakayama, M., Ito, M., Yamauchi, T., Goto, H., Fukata, Y., Oshiro, N., Shinohara, A., Iwamatsu, A., and Kaibuchi, K. Identification of Tau and MAP2 as novel substrates of Rho-kinase and myosin phosphatase. *Journal of*

Neurochemistry, *87*(3), 780-790 (2003).

51. Amano, M., Chihara, K., Nakamura, N., Kaneko, T., Matsuura, Y., and Kaibuchi, K. The COOH terminus of Rho-kinase negatively regulates rho-kinase activity. *Journal of Biological Chemistry*, *274*(45), 32418-32424 (1999).
52. Jiang, S., Wen, N., Li, Z., Dube, U., Del Aguila, J., Budde, J., Martinez, R., Hsu, S., Fernandez, M. V., Cairns, N. J., Dominantly Inherited Alzheimer Network (DIAN), International FTD-Genomics Consortium (IFGC), Harari, O., Cruchaga, C., and Karch, C. M. Integrative system biology analyses of CRISPR-edited iPSC-derived neurons and human brains reveal deficiencies of presynaptic signaling in FTLD and PSP. *Translational Psychiatry*, *8*(1), 265 (2018).
53. Cong, L., Ran, F. A., Cox, D., Lin, S., Barretto, R., Habib, N., and Zhang, F. Multiplex genome engineering using CRISPR/Cas systems. *Science*, *339*(6121), 819-823 (2013).
54. Choi, S. H., Kim, Y. H., Hebisch, M., Sliwinski, C., Lee, S., D'Avanzo, C., and Klee, J. B. A three-dimensional human neural cell culture model of Alzheimer/'s disease. *Nature*, *515*(7526), 274-278 (2014).
55. Quadrato, G., Nguyen, T., Macosko, E. Z., Sherwood, J. L., Yang, S. M., Berger, D. R., Maria, N., Scholvin, J., Goldman, M., Kinney, J. P., Boyden, E. S., Lichtman, J. W., Williams, Z. M., McCarroll, S. A., and Arlotta, P. Cell diversity and network dynamics in photosensitive human brain organoids. *Nature*, *545*(7652), 48 (2017).

56. Sakaue, F., Saito, T., Sato, Y., Asada, A., Ishiguro, K., Hasegawa, M., and Hisanaga, S. I. Phosphorylation of FTDP-17 mutant tau by cyclin-dependent kinase 5 complexed with p35, p25, or p39. *Journal of Biological Chemistry*, *280*(36), 31522-31529 (2005).

57. Chesser, A., Pritchard, S., and Johnson, G. V. Tau clearance mechanisms and their possible role in the pathogenesis of Alzheimer disease. *Frontiers in Neurology*, *4*, 122 (2013).

58. Kowall, N. W., and Kosik, K. S. Axonal disruption and aberrant localization of tau protein characterize the neuropil pathology of Alzheimer's disease. *Annals of Neurology*, *22*(5), 639-643 (1987).

59. Hoover, B. R., Reed, M. N., Su, J., Penrod, R. D., Kotilinek, L. A., Grant, M. K., and Ashe, K. H. Tau mislocalization to dendritic spines mediates synaptic dysfunction independently of neurodegeneration. *Neuron*, *68*(6), 1067-1081 (2010).

60. Schwarz, T. L. Mitochondrial trafficking in neurons. *Cold Spring Harbor Perspectives in Biology*, *5*(6), a011304 (2013).

61. Lin, M. T., and Beal, M. F. Mitochondrial dysfunction and oxidative stress in neurodegenerative diseases. *Nature*, *443*(7113), 787 (2006).

62. Denk, F. and Wade-Martins, R. Knock-out and transgenic mouse models of tauopathies. *Neurobiology of Aging*, *30*(1), 1-13 (2009).

63. Lim, S., Haque, M. M., Kim, D., Kim, D. J., and Kim, Y. K. Cell-based models to investigate Tau aggregation. *Computational and Structural Biotechnology Journal*, *12*(20-21), 7-13

(2014).

64. Tatebayashi, Y., Planel, E., Chui, D. H., Sato, S., Miyasaka, T., Sahara, N. and Takashima, A. c-jun N-terminal kinase hyperphosphorylates R406W tau at the PHF-1 site during mitosis. *The FASEB Journal*, *20*(6), 762-764 (2006).

65. Ikeda, M., Kawarai, T., Kawarabayashi, T., Matsubara, E., Murakami, T., Sasaki, A., and Hasegawa, M. Accumulation of filamentous tau in the cerebral cortex of human tau R406W transgenic mice. *The American Journal of Pathology*, *166*(2), 521-531 (2005).

66. Zhang, B., Higuchi, M., Yoshiyama, Y., Ishihara, T., Forman, M. S., Martinez, D., Joyce, S., Trojanowski, J.Q., and Lee, V. M. Y. Retarded axonal transport of R406W mutant tau in transgenic mice with a neurodegenerative tauopathy. *Journal of Neuroscience*, *24*(19), 4657-4667 (2004).

67. Tatebayashi, Y., Miyasaka, T., Chui, D. H., Akagi, T., Mishima, K. I., Iwasaki, K., and Planel, E. Tau filament formation and associative memory deficit in aged mice expressing mutant (R406W) human tau. *Proceedings of the National Academy of Sciences*, *99*(21), 13896-13901 (2002).

68. Matsumura, N., Yamazaki, T., and Ihara, Y. Stable expression in Chinese hamster ovary cells of mutated tau genes causing frontotemporal dementia and parkinsonism linked to chromosome 17 (FTDP-17). *The American Journal of Pathology*, *154*(6), 1649-1656 (1999).

69. Dayanandan, R., Van Slegtenhorst, M., Mack, T. G. A., Ko, L., Yen, S. H., Leroy, K., and

Lovestone, S. Mutations in tau reduce its microtubule binding properties in intact cells and affect its phosphorylation. *FEBS Letters*, *446*(2-3), 228-232 (1999).

70. Perez, M., Lim, F., Arrasate, M., and Avila, J. The FTDP-17-linked mutation R406W abolishes the interaction of phosphorylated tau with microtubules. *Journal of Neurochemistry*, *74*(6), 2583-2589 (2000).
71. Krishnamurthy, P. K. and Johnson, G. V. Mutant (R406W) human tau is hyperphosphorylated and does not efficiently bind microtubules in a neuronal cortical cell model. *Journal of Biological Chemistry*, *279*(9), 7893-7900 (2004).
72. Imamura, K., Sahara, N., Kanaan, N. M., Tsukita, K., Kondo, T., Kutoku, Y., Ohsawa, Y., Sunada, Y., Kawakami, K., Hotta, A., Yawata, S., Watanabe, D., Hasegawa, M., Trojanowski, J. Q., Lee, V. M.-Y., Suhara, T., Higuchi, M., and Inoue, H. Calcium dysregulation contributes to neurodegeneration in FTLD patient iPSC-derived neurons. *Scientific Reports*, *6*, 34904 (2016).
73. Zhang, Y., Pak, C., Han, Y., Ahlenius, H., Zhang, Z., Chanda, S., Marro, S., Patzke, C., Acuna, C., Covy, J., Xu, W., Yang, N., Danko, T., Chen, L., Wernig, M., and Südhof, T. C. Rapid single-step induction of functional neurons from human pluripotent stem cells. *Neuron*, *78*(5), 785-798 (2013).
74. Wang, Y., and Mandelkow, E. Tau in physiology and pathology. *Nature Reviews Neuroscience*, *17*(1), 22 (2016).

75. Miyasaka, T., Morishima-Kawashima, M., Ravid, R., Heutink, P., van Swieten, J. C., Nagashima, K., and Ihara, Y. Molecular analysis of mutant and wild-type tau deposited in the brain affected by the FTDP-17 R406W mutation. *The American Journal of Pathology*, *158*(2), 373-379 (2001).

76. Reynolds, C. H., Betts, J. C., Blackstock, W. P., Nebreda, A. R., and Anderton, B. H. Phosphorylation sites on tau identified by nanoelectrospray mass spectrometry. *Journal of Neurochemistry*, *74*(4), 1587-1595 (2000).

77. Greer, S., Honeywell, R., Geletu, M., Arulanandam, R., and Raptis, L. Housekeeping gene products; levels may change with confluence of cultured cells. *Journal of Immunological Methods*, *355*, 76-79 (2010).

78. DeTure, M., Ko, L. W., Yen, S., Nacharaju, P., Easson, C., Lewis, J., van Slegtenhorst, M., Hutton, M., and Yen, S. H. Missense tau mutations identified in FTDP-17 have a small effect on tau–microtubule interactions. *Brain Research*, *853*(1), 5-14 (2000).

79. Hong, M., Zhukareva, V., Vogelsberg-Ragaglia, V., Wszolek, Z., Reed, L., Miller, B. I., Geschwind, D.H., Bird, T.D., McKeel, D., Goate, A., Morris, J. C., Wilhelmsen, K. C., Schellenberg, G. D., Trojanowski, J. Q., and Lee, V. M.-Y. Mutation-specific functional impairments in distinct tau isoforms of hereditary FTDP-17. *Science*, *282*(5395), 1914-1917 (1998).

80. Hasegawa, M., Smith, M. J., & Goedert, M. Tau proteins with FTDP-17 mutations have a

reduced ability to promote microtubule assembly. *FEBS Letters*, *437*(3), 207-210 (1998).

81. Kopeikina, K. J., Carlson, G. A., Pitstick, R., Ludvigson, A. E., Peters, A., Luebke, J. I., Koffie, R.M., Frosch, M.P., Hyman, B. T., and Spires-Jones, T. L. Tau accumulation causes mitochondrial distribution deficits in neurons in a mouse model of tauopathy and in human Alzheimer's disease brain. *The American Journal of Pathology, 179*(4), 2071-2082 (2011).
82. Rodríguez-Martín, T., Pooler, A. M., Lau, D. H., Mórotz, G. M., De Vos, K. J., Gilley, J., Coleman, M.P., and Hanger, D. P. Reduced number of axonal mitochondria and tau hypophosphorylation in mouse P301L tau knockin neurons. *Neurobiology of Disease*, *85*, 1-10 (2016).
83. Iovino, M., Agathou, S., González-Rueda, A., Del Castillo Velasco-Herrera, M., Borroni, B., Alberici, A., Lynch, T., O`Dowd, S., Geti, I., Gaffney, D., Vallier, L., Paulsen, O., Káradóttir, R. T., and Spillantini, M. G. Early maturation and distinct tau pathology in induced pluripotent stem cell-derived neurons from patients with MAPT mutations. *Brain*, *138*(11), 3345-3359 (2015).
84. Dixit, R., Ross, J. L., Goldman, Y. E., and Holzbaur, E. L. Differential regulation of dynein and kinesin motor proteins by tau. *Science*, *319*(5866), 1086-1089 (2008).
85. Garg, S., Timm, T., Mandelkow, E. M., Mandelkow, E., and Wang, Y. Cleavage of Tau by calpain in Alzheimer's disease: the quest for the toxic 17 kD fragment. *Neurobiology of Aging*, *32*(1), 1-14 (2011).

86. Chen, H. H., Liu, P., Auger, P., Lee, S. H., Adolfsson, O., Rey-Bellet, L., Lafrance-Vanasse, J., Friedman, B. A., Pihlgren, M., Muhs, A., Pfeifer, A., Ernst, J., Ayalon, G., Wildsmith, K. R., Beach, T. G., van der Brug, M. P. Calpain-mediated tau fragmentation is altered in Alzheimer's disease progression. *Scientific Reports*, *8*(1), 16725 (2018).